Universiteit Utrecht

Faculteit Bètawetenschappen

A preshower experiment

On the use of a preshower calorimeter for the distinction between pions and electrons

Bachelor Thesis

René Moesbergen

Natuur- en Scheikunde

Supervisor:

Prof. Thomas Peitzmann
Institute for Subatomic Physics

June 12, 2019

Abstract

In this thesis we will discuss a preshower calorimeter, a counting calorimeter based on the FoCal. To study the possibilities of this detector we have used a GEANT3 simulation, which was developed for the FoCal.

To study this we looked at the distribution of the number of hits that were detected by the active layers. At first we looked at a case where every particle was just registered as one single hit, here we saw that the all electrons shower, in contrast with the pions of which only a small fraction showered. After that we incorporated a charge diffusion, where one particle can excite multiple particles, this led to a broadening of the hit distributions and with it a severe drop in accuracy to discriminate them from eachother. After that we looked how a raising in discriminator value looked like, meaning that a pixel needs more charge before it gives a signal. We found that this only gave us again lower accuracies. Lastly, we looked at the impact of the geometry, for this we found that the accuracy with which we can discriminate electrons from pions increases heavily the more layers we add.

In short, it seems to be very promising to use a preshower calorimeter to discriminate electrons from pions.

Contents

1 Introduction **1**
1.1 Particle Interactions with matter . . . 1
1.1.1 Electromagnetic interactions of charged particles . . . 1
1.1.2 Electromagnetic interactions of photons . . . 2
1.1.3 Strong interactions . . . 4
1.2 Electromagnetic Calorimeters . . . 4
1.3 The preshower calorimeter . . . 5

2 The Preshower Simulation Framework **7**
2.1 The Input . . . 7
2.2 The Simulation Phase . . . 7
2.3 The Data Reconstruction Phase . . . 9

3 Results **10**
3.1 Choices of Input . . . 10
3.2 Hit Distributions . . . 11
3.2.1 Pure Hits . . . 12
3.2.2 Charge Sharing . . . 15
3.3 Discriminator settings . . . 19
3.4 Configuration settings . . . 22
3.5 General Remarks . . . 26

4 Conclusion **27**
4.1 Further Research . . . 27

A Distributions for different geometries **29**

1 Introduction

In this thesis, we will investigate the use of a preshower calorimeter to discriminate electrons from pions. This is done using a calorimetry technique, as explained in the sections below. The main difference, however, will be that only a few layers will be used, instead of a full detector of over twenty layers, as in the Forward Calorimeter (FoCal), on which the geometry is based.
This study is of particular interest in the development of a proposed detector for a new LHC experiment [5]. This experiment will open a way to study fundamental physics in a way that could not be done before. The preshower detector will be on outer layers, to which it is referred as a SHower Pixel Detector (SPD). They made the assumption that the contamination from pions will be small due to the ratio in interaction lengths. To study this assumption, we will first discuss how we a calorimeter works, then we will introduce the preshower detector and its looks. In the next chapter we will discuss the code that was used to perform the simulations and in the last chapter we will discuss the results we found.

1.1 Particle Interactions with matter

In order to detect particles, they must undergo some interaction with the material of the detector. In this section we will discuss briefly these interactions. Generally speaking there are three categories of interactions:

- the electromagnetic interactions of charged particles,
- the electromagnetic interactions of photons,
- the strong interactions.

1.1.1 Electromagnetic interactions of charged particles

For a relativistic charged particle the main loss of energy is the loss by ionizing the atoms within the medium, which is primarily due to the Coulomb force. [2, 3, 6] For a single particle with velocity v and charge q, in units of e (the charge of an electron), traversing a medium with atomic number Z and number density n, one can express the ionization energy loss by the Bethe-Bloch equation;

$$\frac{dE}{dx} \approx -4\pi\hbar^2\alpha^2 \frac{nZq^2}{m_e\beta^2}\left[\ln\left(\frac{2m_e c^2\beta^2\gamma^2}{I}\right) - \beta^2\right] \tag{1}$$

where $\hbar$ is Planck's constant divided by 2π, α is the fine structure constant, c is the speed of light, m_e is the mass of the electron, $\beta = v/c$, $\gamma = \left(1-\beta^2\right)^{-1/2}$ and I is the mean ionization potential of the atom averaged over all electrons, which can be further approximated by $I \approx 10Z$ eV for $Z > 20$ [2].It is common to rewrite this expression into one containing the number density, defined as $n = \rho/(Am_u)$, where ρ is the mass density of the material, A the number of nucleons in the atom, and m_u is the atomic mass unit. This gives

$$\frac{1}{\rho}\frac{dE}{dx} \approx -\frac{4\pi\hbar^2\alpha^2}{m_e m_u}\frac{Z}{A}\frac{q^2}{\beta^2}\left[\ln\left(\frac{m_e c^2}{5Z}\right) + 2\ln\left(\beta\gamma\right) - \beta^2\right] \tag{2}$$

From this equation we see a few things, first of all we have a constant factor, which obviously does not change upon changing the material and/or the incoming particle. Furthermore, we notice a term $\frac{Z}{A}$, which is the fraction of protons inside the nucleus. For most atoms, at least for those above $Z > 20$, which was needed to approximate I, this fraction $\frac{Z}{A}$ is approximately constant and fluctuates around $0.4 - 0.5$. We also see a factor q^2, which is just a factor describing how well the electrons in the medium 'feel' the passing particle.
Furthermore we can see that the energy loss is primarily dependent on the density of the medium and not the element number of the medium, since $\frac{1}{\rho}\frac{dE}{dx} \sim \ln(Z)$, which increases far more slowly for a large element number Z. Last but not least we see that there is a dependence on $\beta\gamma$. At low momenta, the function drops very fast due to the $\frac{1}{\beta^2}$ term, at high momenta the functions rises slowly due to the logarithmic dependence. Between these two behaviours there is a so called MIP, a minimum ionizing particle, which refers to the minimum of the ionization energy loss curve. This behaviour is plotted in figure 1.
This is however not the entire story, for there are other ways a charged particle can lose its energy. One of which being the so called Bremsstrahlung, which is particularly important for relativistic electrons and

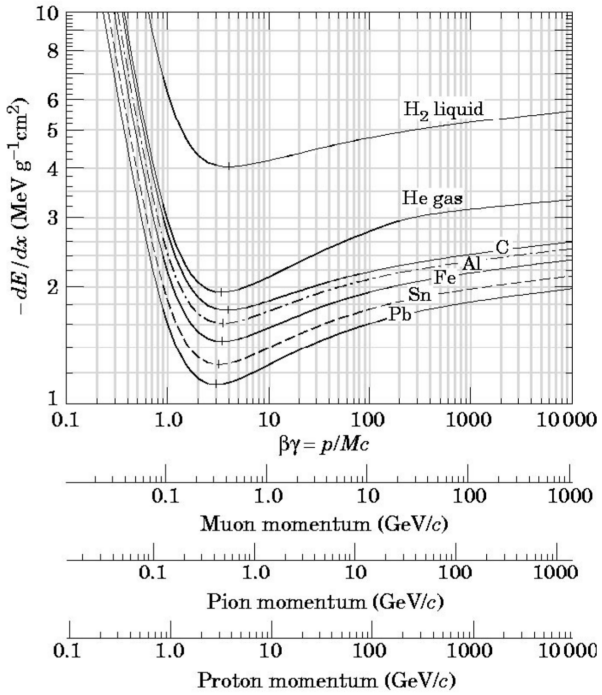

Figure 1: Ionization energy loss for muons, pions and protons in different media [3]. Here we clearly see that there is first a steep drop, then an minimum ionizing energy and in the end a slowly increasing

positrons. [2, 3, 6] In this process a particle 'collides' with another electrostatic field primarily due to the nuclei. Upon entering this electric field, the particle will be accelerated and decelerated as it passes through this field, leading ultimately to the loss of energy through a photon.
One can find that this energy loss is proportional to E/m^2[6], this in contrast to the logarithmic dependence of the momentum for the energy loss in the ionization process. This results for electrons and positrons at high energy scales in a complete dominance of energy loss by Bremsstrahlung. The mass dependence, however, results for heavier particles in a dominance of a ionization losses, unless you go, obviously, to even higher energies.
The last electromagnetic interaction of charged particles we will discuss is Cherenkov radiation.[2, 3] Whenever a charged particle transverses a dispersive medium of refractive index n, the atoms in the vicinity of the particle will become polarized. If the particle passes slowly, the disturbance caused by this particle will elastically relax back into equilibrium. When the particle, however, transverses the medium with a velocity high enough, the polarized atom cannot respond fast enough to relax back to its original position. And thus it is left with an energetic disturbance, which means it will emit a photon to get rid of this extra energy.
One can work out the effect of this Cherenkov radiation. For this a particle has to exceed the velocity of light in that medium, since that is the limitation at which the atom can respond on the passing particle. Thus the particle has an velocity of $c/n < v < c$ with c the speed of light in vacuum. This yields an angle θ, at which the wave front travels. This angle is given by $\cos\theta = \frac{c}{nv}$[3].
Apart from these electromagnetic interactions, there are some other left, like the Bhabha radiation and positron annihilation. [3] These processes, however, occur even far below the critical energy, where ionization is the dominant process. This means that for our understanding of this paper it is enough to see those as some higher order corrections and not as primary processes and we will therefore not discuss them here.

1.1.2 Electromagnetic interactions of photons

Although we saw that it were only the charged particles that interacted via the electromagnetic force, there is one 'special' neutral particle. This is not a particle, which interacts with other particles via the electromag-

netic force, but it is the particle that carries the electromagnetic force. It is called a photon. This particle has been mentioned in the previous section, where we spoke about the interactions of charged particles. In all cases a photon is involved in those interactions, but it is also possible to fly free in space and in doing so it has a chance to interact with the charged particles it encounters.
Here we shall discuss the following processes; Rayleigh scattering, where the photon is unaffected in energy. Compton scattering, where a photon scatters off a charged particle, while in the process liberating it. The photoelectric effect, where a photon is absorbed by and liberates an electron. And the pair production process, where a photon is converted into two particles.
First of all, a photon can undergo Rayleigh scattering, which is just an elastic scatter off an electron inside the medium. This process leaves the energy of the photon, however, unchanged and such there cannot be created any other particles. This means that it only affects the direction the photon moves in[6].
Whenever such a photon, however, carries just the exact amount of energy such that an electron can excite from one orbital to another, this photon is absorbed by the electron, transferring the energy to the electron. [4] This electron then excites to the higher state. This is, however, not the preferred state of the electron and it can get rid of this extra energy by either relaxation or emitting another photon. Whenever the photon is even more energetic, such that the electron gains more energy than needed for the highest orbital, the electron can still absorb the photon and by doing so it is liberated from the nucleus. This process is called the photoelectric effect. In doing so, one effectively transforms one photon into a slightly less energetic electron.
Whenever such a freed electron has enough energy to ionize other atoms, we call it a delta electron. This term is not solely used for electrons liberated by the photoelectric effect, but also by other processes such as the previously described ionization process and further on explained Compton scattering. The photoelectric effect is, however, the main producer of these delta rays.
Next a photon can scatter off a charged particle, like with Rayleigh scattering, but instead of an elastic scatter, energy and momentum is transferred from the photon to the charged particle. [6] For this we treat the particle as free, meaning that any binding energy will be neglected, since it is sufficiently small compared to the energy of the photon. For a photon, which is traveling through a 'normal' medium, these charged particles are electrons, so we will use the constants that describe this particle.
With $\zeta = E_\gamma / m_e c^2$, the relation between the scattering angle of the electron and the photon, ϕ and θ respectively, which are relative to the direction of the incoming photon, is given by:

$$\cot\phi = (1+\zeta)\tan\frac{\theta}{2} \text{ for } \theta \neq 0 \tag{3}$$

$$\phi = \theta \text{ for } \theta = 0 \tag{4}$$

Using QED one can calculate the cross section, which is related to the chance a process takes place, from the Klein-Nishina relation, namely:

$$\frac{d\sigma}{d\Omega} = \frac{r_e^2}{2}\frac{1+\cos^2\theta}{\left(1+\zeta\left(1+\cos^2\theta\right)\right)^2}\left[1+\frac{\zeta^2\left(1+\cos^2\theta\right)^2}{\left(1+\cos^2\theta\right)\left(1+\zeta\left(1-\cos\theta\right)\right)}\right] \tag{5}$$

where r_e is the reduced Compton wavelength for an electron (0.386 16 pm). If one were to plot equation 5 as a function of the angle, one would find that for energies in the MeV range and above, the cross section is almost flat in the backward direction, thus angles $\theta > \pi/2$ and increases to the maximum at $\theta = 0$. Implying that the photon, which travels through a material, will most likely keep traveling in (approximately) the same direction. And with it, it takes an electron, which must travel in the forward direction as well to conserve energy and momentum. At last we can see from equation 3 that a higher energetic photon, leads to an electron traveling in a more forward direction.
One can also calculate how much energy is lost per interaction, which is

$$E_{lost} = E_\gamma \frac{\zeta(1-\cos\theta)}{1+\zeta(1-\cos\theta)}. \tag{6}$$

This implies together with the previous knowledge that the photon will most likely not deflect much from its incoming trajectory, it is more likely that a photon will lose it energy through many low momentum transfers than through one single high momentum transfer.
Last, but definitely not least, a photon can create a pair of an electron and a positron. [2, 3, 6] For this to happen, however, it needs at least an energy larger than the restmass of one electron and one positron, which is approximately twice the restmass of an electron. Furthermore it needs to be in the electromagnetic field of a charged particle, which can act as a scattering partner to conserve energy and momentum. In a normal material, this means the nucleus. The electromagnetic field caused by them is however mostly shielded by the orbiting electrons, which becomes more important for higher energies. These cross sections can be calculated using [6]

$$\sigma = r_e^2 \frac{Z^2}{\alpha}\left(\frac{28}{9}\log\frac{2h\nu}{m_e c^2} - \frac{218}{27}\right);\ m_e c^2 \ll h\nu \ll Z^{-1/3} m_e c^2/\alpha \tag{7}$$

$$\sigma = r_e^2 \frac{Z^2}{\alpha}\left(\frac{28}{9}\log 183 Z^{1/3} - \frac{2}{27}\right);\ h\nu \gg Z^{-1/3} m_e c^2/\alpha \tag{8}$$

with Z the atomic number of the atom, h Planck's constant, ν the frequency of the photon, α the fine structure constant and $r_e = e^2/m_e c^2$ representing the classical electron radius.
We see from this that saturation appears for higher values of Z more quickly. This and the Z^2 dependence give us the insight that the pair production process is a dominant process for these higher Z materials.
From momentum and energy conservation, one can argue that it is the most likely that the electron and positron carry approximately the same amount of energy and travel in almost the same direction as their mother-photon.

1.1.3 Strong interactions

The last category of interactions are the strong interactions. [2, 3] For hadrons, particles that consists quarks, the most important interactions are due to the strong force, which is not dependant on the charge, such as the previously discussed electromagnetic interactions. These interactions can as well result into elastic and inelastic interactions, but with increasing energy there is an increasing amount of possible inelastic interactions. Of these many result into one particle that will create multiple other particles.
The probability that such hadron-nucleus interaction will occur whenever the hadron travels through a material can be characterized by the collision length $\lambda = 1/n\sigma$, where n is the number of nuclei per unit of volume and σ is the cross section, the chance of occurring. This represents the mean distance a particle can travel, before an interaction occurs, thus a larger collision length means that it is less likely to happen. As an example, the collision length for iron is $\lambda(Fe) \approx 17\,\text{cm}$, compared to a collision length for an electromagnetic interaction, called the radiation length, of $1.8\,\text{cm}$[3].

1.2 Electromagnetic Calorimeters

As we can see in the previous section, there are many ways a high energetic particle can lose its energy and in the process, either create new particles, which is the case for i.e. pair production or brehmsstrahlung, or excites particles within the material (primarily electrons), which is the case for i.e. the the photoelectric effect and ionization. This will result in an electromagnetic shower, where one typically starts with a multi-GeV electron or photon. [6, 7]
This photon will most likely transform into an electron and a positron with both approximately the same energy meaning we will still obtain a multi-GeV electron. These particles will lose their energy primarily through Bremsstrahlung, where most of the photons will have a relatively low energy and are absorbed by electrons within the medium by Compton scattering and the photoelectric effect.
The photons that have an energy in the MeV region will lose their energy by pair-production. Whenever those created particles have an energy that is high enough those will again emit photons through Bremsstralung, which has a chance to create new electron-positron pairs. This is called an electromagnetic shower.
As the shower continues, the average energy per particle drops and more and more particles are being absorbed, meaning the shower will be stopped. This basically means that all the energy from the incoming

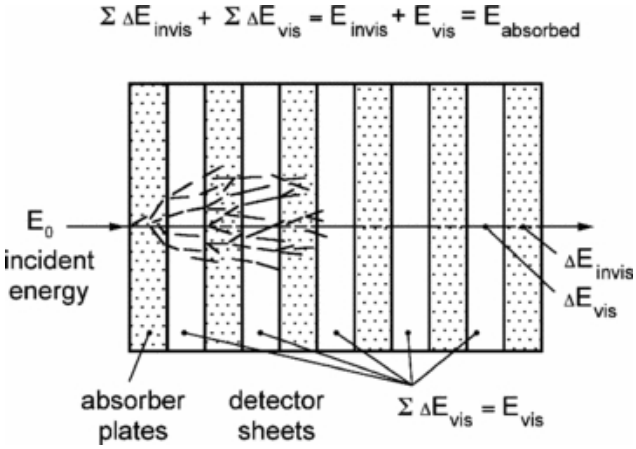

Figure 2: A schematic view of a sampling calorimeter. An incoming particle creates new particles, which are then being measured in the detecting sheets.

particle is transferred to the material it has passed. A calorimeter basically measures this energy, and by adding all the energies that were deposited, one can determine the energy of the incoming particle. To do this, one can use two kinds of calorimeters, either a homogeneous or a sampling calorimeter. [7]
A homogeneous calorimeter has as main advantage that the material used as the absorber for the shower is the same material as the one used for the measurements, leading to an optimal energy resolution. The materials that are used for this, however, are very expensive and have long radiation lengths.
On the hand there exist sampling calorimeters, as given in figure 2, these are built of altering layers of passive absorbers and active read-outs. Here one creates the shower primarily in the passive layers, while a part of the energy is measured in the active layers. This means that one can choose the material for one purpose only, giving less concessions in the other job. For example, one does not have to be able to get the energy that is deposited in the absorbers, thus makes the choice solely on the density of the material. This means, however, that only a fraction of the energy is measured and thus has a lower energy resolution.
Besides measuring the energy that is deposited in the active layers, one can also measure the number of passing particles, since a more energetic shower creates more particles than a low energetic ones, since it takes more particles to reduce the average energy per particle below the critical energy, where the particles are being absorbed. This is what for the FoCal (Forward Calorimeter) does.

1.3 The preshower calorimeter

This calorimeter is built using altering active and passive layers. [7] These passive layers, made out of tungsten, have a thickness of approximately one radiation length, which is ca. 3.5 mm. The active ones, made out of silicon and electronic circuits, have a thickness of a few micro meters.
In older prototypes, a type of Monolithic Active Pixel Sensor (MAPS) was used for these active layers, the MIMOSA32 chip. This chip has a thickness of 30 µm and a area of 19.52 mm × 20.93 mm. Inside this area, there is an area of 19.2 mm × 20.2 mm, containing 640 × 640 pixels.
In the Focal itself, each layer consist of one block of tungsten with an area of 5 mm × 5 mm and four active layers, places next to each other, giving an effective area of approximately 4 mm × 4 mm. The complete FoCal consists of 24 of these layers, to reduce costs, however, in the end some of the active pixel sensors have been excluded.
The simulated preshower calorimeter, is based on this FoCal, and thus will have the same structure. The main difference will be that, instead of the full 24 layers, it will have just a few. This means that we can easily use the simulations that were built for the FoCal prototype to study this preshower calorimeter.
This preshower calorimeter will be used for identification of electrons and photons with a momentum higher than 500 MeV, so we have chosen to do the simulations for electrons and pions with a momentum of $1-50$ GeV. With these simulations we will study the behaviour of the number of activated pixels per incoming particle and how they are distributed for both the pions and the electrons. Next we will try to find a way to optimize

the calorimeter, such that these distributions have as less overlap as possible. To do this, we will first try to change the condition at which a pixel is activated. Apart from that, we will as well alter the number of layers.

2 The Preshower Simulation Framework

The used simulation framework is written for the ALIROOT environment, which is based on the C++ object oriented language. [1] This environment, which was created at CERN, adds varying functionalities needed to deal with eg. simulations, big data processing and statistics. Of particular interest for this study is the classes that are added by the GEANT-interface, which offers direct control over the GEANT-framework, used to run the Monte Carlo simulations.
The code can be split into two phases, namely the simulation phase, executed by the GEANT3-program, and afterwards the data reconstruction phase, executed by the FocalPixelManager class. For these phases one need some input files containing things such as the geometry of the detector and the primary particles.

2.1 The Input

geometryfile.txt

First of all one has to define the geometry of the simulated experiment, this has to be done in the "geometryfile.txt". Within this file, multiple aspects of the geometry can be described. In the first line, the labframe is created. Next one can define the used materials. Using one of these materials one can shape it in its desired form, which can be used to build bigger structures and eventually be stacked in layers to create the complete detector. One can choose here to misalign those layers and set their sensitivity individually. In addition, the cut-off energy for different particles and the step size parameters can be defined.

primaryfile.txt

The next thing one has to describe is the particle one uses for the simulation. This can be done in the primaryfile.txt by parameters like particle type, origin and origin/momentum, which can be chosen to be fixed or distributed according to some predefined distributions.

analysisfile.txt

The third and last file contains the information about the pixel structure of the chips inside the detector. This information will be used after the simulation to convert the energy deposition into excited pixels, with or without any diffusion. This diffusion can be changed by some parameters in the FocalPixelManager class.

Other Parameters

Beside these input-files, there are also some other parameters and options one needs to change in the code itself.
Firstly one can set the drawing options after the simulation run. By default it only shows the detector construction, but there are some useful predefined drawing functions. One can turn these on/off by (un)commenting them in the EndSimulation function inside the FocalMCapplication class, see section 2.2. You can draw things like the tracks, with or without photons, or the hits, for just one or all layers.
Furthermore, you can determine how the induced charge on the chip diffuses over it, this can be done by the use of three parameters defined in the FocalPixelManager class. The first parameter, edepchargefactor, converts the deposited energy into an number of electrons, which is a measurement for the energy needed to ionize the pixel by one electron. The second parameter, chargeDistributionFactor, describes the width of Gaussian distributed charge diffusion. If one gives this the value of zero all charge will be bound to the single pixel that was hit by the particle. The third and last parameter, defaultdiscriminatorelectrons, is a measurement for the discriminator above which amount of electrons the pixel will be turned on. This last parameter has to be an integer, contrary to its definition as a double.

2.2 The Simulation Phase

The code starts (obviously) with a simulation, this is done, as told before, using the GEANT3 framework. Before this simulation can be started, an instance of FocalMCapplication is created, which acts as the interface for communication with the GEANT3 program.

Upon creation of the FocalMCapplication instance five other object are created;

- FocalMCstack: The first object created is an FocalMCstack-instance, this manages the particles that are used and/or created by the GEANT-simulation, so the primary and secondary particles.
- FocalHitGenerator: The following object, which is an instance of FocalHitGenerator, checks at every Monte Carlo simulation, whether there was any energy deposited in one of the sensitive volumes, which are compressed in an array containing SensitiveVolume objects. If this is the case, then this energy deposition is saved as a FocalHit object, containing information like the position and energy deposition of the particle.
- DetectorConstruction: The next object, an instance of DetectorConstruction, reads the geometry text-file and creates the corresponding geometry, which will be saved as an ALIROOT GeoManager instance.
- PrimaryGenerator: Furthermore there is a PrimaryGenerator instance, which reads your predefined primary particle text-file and generates the associated set of primary particles. It basically converts the text-file into an array of TParticle objects, which contain information like the flavour and position. These are thereafter pushed onto the previously defined FocalMCstack.
- TRandom: The last object is an instance of TRandom, which basically just generates random values, which are handed over to the GEANT simulation upon initialization.

Now that these objects are created, the code can start its initialization phase, where it will construct the detector and the sensitive layers. These objects, the DetectorConstruction and FocalHitGenerator, are together with the FocalMCstack and TRandom objects handed to the GEANT program. Furthermore the physics section of the GEANT program is initialized, which it will use to determine things like the cross-section of the particle and the needed physical relations.
Now that the program has initialized the experiment, it can run the simulations, which starts with the generation of the primary particles, which are saved in a particle array. Now the GEANT program will run its simulation, which will use the functions in the FocalMCapplication class. These are, in this specific order;

- BeginEvent: This basically does nothing.
- GeneratePrimaries: This function pushes the particles that are created for that specific event onto the FocalMCstack object.
- BeginPrimary: This again does nothing.
- PreTrack: This generates a so called TGeoTrack object, where basically the tracks of the particles are stored. These tracks are only used to draw the tracks just after the simulation and are not saved in a e.g. root file.
- Stepping: This function controls the Monte Carlo simulation, since it is called at every step within this. First of all, this function checks whether the energy deposition was within a sensitive volume. If this will be the case, the track position and time will be saved. Furtermore the tracks are saved to the previously defined track.
- PostTrack: This just adds an extra track.
- FinishPrimary: This concludes this primary of this event. If there are no primaries left it will simply continue to the next function. If there are still other primaries left, it will return to the BeginPrimary function and run the next primary particle in this event.
- FinishEvent: This function ends the event, which basically means the same as the for the primaries, if there are still events left it will just return to the BeginEvent function, otherwise it will continue to the EndSimulation function.
- EndSimulation: This function terminates the simulation. It will write the hits that were saved in the stepping phase to a txt- and root-file. Furthermore it will write the sensitive volumes to a root file, since they will be needed later on, and the primary particles are written to a txt-file, since one could possibly need them later on in the analysis procedure. At last there are some drawings one can show.

2.3 The Data Reconstruction Phase

Now that the simulation has ended, we know the positions and energy depositions of the particle hits the active layers. From this we can now deduce whether a particle excited a pixel or not. To perform this, an instance of the FocalPixelManager is created, which governs the conversion of the FocalHit objects into FocalFrame objects, which contains the number of pixels that gave a signal in a certain chip and time frame. First of all, the program loads the FocalHit objects from the corresponding ROOT-file and reads the predefined parameters from the analysis file. Next one can choose to translate the hits to the positive quadrant to make it easier to calculate which pixel was hit, because one can start counting from bottom left as the (0,0) pixel. This is done by the TranslateHits function.
After the determination of the hit pixels, the code will call the CostructFrames function, which first loops over all events, all chips and all time frames, which are determined by the readout time of the detector. For all FocalHit object it checks whether the event number, the chip and the time frame matches. If this is the case the energy deposition will be converted to a charge, which is than, according to a two dimensional Gaussian distribution, distributed over the chip around the hit position. Next the charge over twenty-five pixels around the hit pixel are calculated and added to a FocalFrame object, to collect all the charges that are present on every pixel. Subsequently noise can be added according to a binomial distribution. At the end of this function there is a discriminator function, which will add the different charges at the same pixel to a final charge. Furthermore it checks if the total charge is above a certain discriminator setting, if so nothing happens, if the condition is, however, not met, that frame will be removed from the array. This gives in the end an array containing all the pixels that would have given a signal in a 'normal' experimental set-up. One can rewrite these criteria as

$$Q_{ind} = C \cdot E_{dep} \tag{9}$$

$$Q_{pixel} = \int_{pixel} \frac{Q_{ind}}{2\pi\sigma^2} \exp\left(-\frac{(x - x_{hit}) + (y - y_{hit})}{2\sigma^2}\right) dA \tag{10}$$

$$Hit_{pixel} = \begin{cases} 1, & \text{if } Q_{pixel} \geq \alpha \\ 0, & \text{if } Q_{pixel} < \alpha \end{cases} \tag{11}$$

where E_{dep} is the energy deposited by the passing particle, C is the conversion factor, Q_{ind} is the induced charge, $(x, y)_{hit}$ are the coordinates the particle has passed the material, σ is the charge diffusion width, Q_{pixel} is the total charge in one pixel, α is the discriminator value, and Hit_{pixel} is a logical value, whether the pixel gives an output or not.

3 Results

3.1 Choices of Input

As told, the goal of this thesis is to investigate the opportunity to use a FoCal-like detector to discriminate electrons from negatively charged pions in a relatively low momentum range of a few GeV/c. Because of this, the simulations will run at the following momenta, 1, 2, 5, 10, 20 and 50 GeV/c, to see how the behaviour of the shower changes depending on the momentum. Furthermore we have chosen to change the momenta instead of the energies, since the geometry of the full detector allows the calculation of the momentum and not the energy.

Furthermore we have chosen the geometry to consist of two layers of tungsten, where the first tungsten layer has a thickness of 0.4 cm and the second one a thickness of 0.8 cm, where after the first and the second layer two active silicon layers are present. Such that the first and second layer of tungsten correspond to approximately one and two radiation lengths respectively, as given in figure 3. This geometry is chosen to be a two layer system, because we minimize the duration of the simulation and analysis in this case. We do, however, not expect that the general behaviour of the i.e. hit distributions change the more layers you add, so we can try to optimize a way to distinct the electrons from the pions without dealing with either too much data or a very long simulation. Whenever we found a good way to discriminate those, we can try that technique to further increase the certainty, when adding more layers.

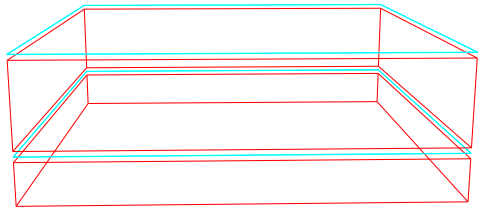

Figure 3: The geometry of the detector, first an tungsten block with a thickness of 0.4 cm, an active layer of 2.8 µm thick silicon, a second block of tungsten with a thickness of 0.8 cm, and lastly another silicon layer.

For these active layers we have chosen the layout for the MIMOSA23 chip, which has been used for the FoCal in the past. These chips consist of 640 x 640 square pixels, of which each has an area of 30 µm x 30 µm. [1, 7] In addition, the readout time of such a chip is 640 µs.

Charge Diffusion Parameters

Regarding the choice of the parameters for the induced charge diffusion, we will look at two different cases. First of all, we will look at the case, where every particle passing the chip will only leave a charge on the exact position it passed. This means that all of the charge is confined within the same pixel and thus one particle can only excite one pixel, meaning that if two particles hit the same pixel, we see it only as one. This is, however, not quite realistic, since the charge that is induced on a chip will not stay focused at one position, but it will flow over the chip, resulting in the excitement of multiple pixels instead of just one.

To check our model for the charge distribution and determine our parameters we will try to fit the model to previously measured cluster size data, where a cluster is defined as a group of neighbouring pixels, but we try to approach this by looking at just one particle that passes through. This experimentally determined cluster size can be found in figure 4, originating from the PHD thesis of Chunhui Zhang [7]. We will use our Gaussian approximation for the charge sharing and try to find the parameters by trial and error to match the data as good as possible. Here it is important that one chooses a distributed beam, since it is of importance to generate hits all over the pixel, not just in one corner. This would namely mess up the results, since it is the position within the pixel that primarily defines how many and which pixels are excited.

This charge diffusion, which we, as told, approximate by a Gaussian distribution, can be described by two parameters, namely the conversion factor for energy to charge governing the area of the function, which is equivalent to changing the charge discriminator, and the diffusion factor governing the width of the Gaussian. To estimate these parameters, we will first make a rough guess and afterwards one can fine tune these. One can easily guess the width value of the Gaussian, since this $\sigma \approx \frac{L}{4}\sqrt{\langle N \rangle}$, where L is the width of one pixel and $\langle N \rangle$ is the average cluster size. One can make this guess, since the square root of the average cluster size is the average number of excited pixels in one dimension, this means an average width of $L\sqrt{\langle N \rangle}$. This is approximately all charge, meaning that this is approximately equivalent to, in a Gaussian approximation, a width of 4σ. Thus one finds above estimation. In our case this would be $\sigma = \frac{3 \cdot 10^{-5}}{4}\sqrt{\langle 4 \rangle} \approx 15\,\mu\text{m}$, where

the average cluster size was estimated from the experimental data for the MIMOSA23 chip [7], of which the plot can be found on the left side of figure 4.
Once one has estimated the charge diffusion width, one has to determine the energy to charge conversion factor and/or the discriminator value. In fact only the ratio of those two that is important, since both are linear correlated to each other, as we can show as $\int_{x_{min}}^{x_{max}} C \cdot p(x)dx > \alpha$, where C is the energy to charge conversion factor, $p(x)$ is the charge distribution in one dimension and α is the discriminator value. As we can see from this relation, and since C is not dependant of the position, we can just take C out of the integral and since it is positive we can take it to the right hand side of the equation without flipping the inequality, we find a $\frac{\alpha}{C}$ ratio. In this simulation the C conversion factor should be approximately 10^6 higher than discriminator value. One should at least obtain a cluster size distribution where there are just a few peaks visible in the lower part of the cluster size distribution.
Once these estimations have been made and one obtains a similar cluster size distribution plot as the experimentally found data, one can try to optimize the parameters to find an even better fit. This can be done by slowly changing the parameters one by one. There are basically four different permutations one can make, namely either raising or lowering one of the two parameters. The easiest to imagine is the change of the width of the peak, an increasing width for example yields in a more spread out charge and thus more pixels are activated, meaning that the distribution will shift to higher cluster sizes and a smaller width equivalently leads to a shift to the lower sizes of the distribution. The charge at one pixel, however cannot decrease any lower and will subsequently rise. Changing the discriminator leads for a higher discriminator as well to a shift to lower cluster sizes, however unlike the change of the charge diffusion parameter this one does not give a rising peak of a cluster size of one, since there are also cases that are just above the discriminator value and are thus suppressed through an increased discriminator. A lower discriminator leads to a shift of the distribution to larger cluster sizes, similar to the change in charge diffusion, with the difference that if some hits are suppressed by the high discriminator value, they will slowly again be included, leading to a slower shift of the peak at a cluster size of one. This effect can also be seen in figure 11.
Following these steps we were able to reproduce the cluster size distribution as shown on the right hand side of figure 4. For this we found the following parameters, for the energy to charge conversion factor $C = 10^7$, a discriminator value of $\alpha = 14$ and a charge diffusion factor of $\sigma = 2.25 \cdot 10^{-3}$. As we see in that figure, however, it does not have exactly the same shape, but it is a good resemblance. We did not spend any more time in improving it any further, since this cluster size distribution was made with an older and thus slightly outdated chip, meaning that the chip used nowadays does probably not show exactly the same distribution. Furthermore it goes beyond the scope of this thesis to find an exact description of the charge sharing model, so this found distribution is probably good enough for our goal.

3.2 Hit Distributions

To obtain a way of discriminating electrons from pions using a calorimeter we have to find a property that is different for both showers. Now we have seen in section 1 that a pion will not start an electromagnetic shower immediately, however, it can decay in a neutral pion, which decays into two photons and such an electromagnetic shower is started. We, however, also saw that the chance of such hadronic interaction has a very small chance of occurring. This gives rise to the idea that we may be able to use the easiest method one can apply to a digital calorimeter, just counting the number of hits.
This was done by using the code described in section 2.2, where we used for the electrons and the pions respectively $5,000$ and $50,000$ events per energy. From this simulation we obtained a number of hits per event, which will form a distribution. We do expect that the amount of hits for the electrons to be higher than the pions. To explain their behaviour we will first look at the distributions of hits without any charge diffusion, because we may not be able to interpret the hit distributions well, because when we look at the cluster size distributions in figure 4 we see that the cluster size has quite a odd looking behaviour, it is not a simple Gaussian or something like that.
To determine our errors we have assumed that every number of hits will follow a binomial distribution. This will give a variance of $\sigma_n^2(x) = n_{events}p(x)(1-p(x))$, where n_{events} is the number of trials, thus number of events measured, $p(x)$ is the chance of finding that number of hits and x is the number of hits. We want to know, however, the chance of finding those number hits, we estimate this by $p(x) = n(x)/n_{events}$, where $n(x)$ is the number of events at that number of hits. This results in $\sigma_n^2(x) = n_{events}\frac{n(x)}{n_{events}}\left(1 - \frac{n(x)}{n_{events}}\right) =$

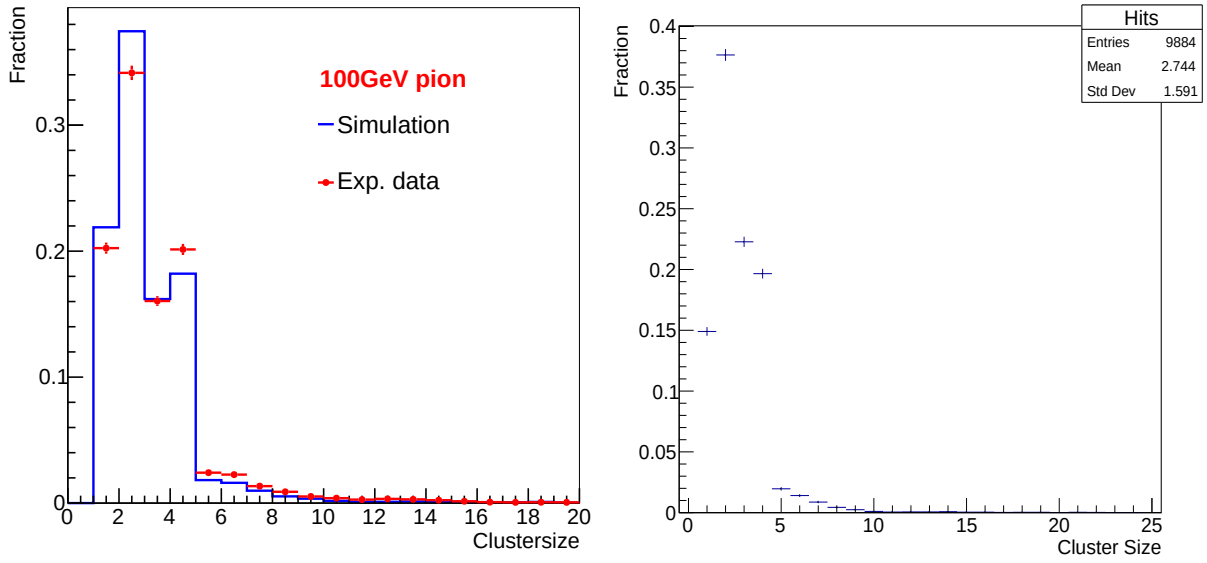

Figure 4: The fraction of appearance for a specific cluster size, which is the number of pixels that turned on due to the hit of one charged particle, in this case a 100 GeV pion. On the left side one sees the original data from a previous experimental run and on the right is the reproduction of that data with our used simulation, where we chose a energy to charge factor of 10^7, a charge diffusion factor of $\sigma = 2.25 \cdot 10^{-3}$ (in cm) and a discriminator value of 14.

$n(x)\left(1 - \frac{n(x)}{n_{events}}\right)$, it is however more useful to look at the fraction of occurrences rather than the absolute number of occurrences, this can be simply done by dividing the standard deviation by the total number of measured hits. Our final estimate of the standard deviation becomes then:

$$\sigma_p(x) = \frac{1}{n_{events}} \sqrt{n(x)\left(1 - \frac{n(x)}{n_{events}}\right)} \tag{12}$$

3.2.1 Pure Hits

First of all we plotted the hit distributions for the 2, 5, 10 and 50 GeV cases in figure 5 to see what these distributions look like. As we can see in the distributions of hits for the electron, on the left hand side, we see that one incoming electron generates up to approximately 2000 hits. This means that this one electron must be showering, since one particle can only excite one pixel in every layer of silicon, thus a non showering particle would generate at most 2 hits. This, however, is exactly what we see on the right hand plot, where the distribution of hits for the pions is shown. This means that those have not yet undergone any interaction, which is logical, taking into consideration that the pions have to undergo a hadronic interaction, before any electromagnetic shower can occur and with it the large collision length for strong interactions.
Furthermore, we can see that there is a possibility the pion can decay or be transformed by the strong interaction into a electromagnetic particle, which can in its turn create an electromagnetic shower. This shower, however, does not contain all the energy the incoming particle had, but rather a fraction of it, resulting in a smaller electromagnetic shower. This has as well a wider range, for example, the electron shower for 50 GeV has a range from about $10 - 2000$ hits, while the pion shower has at the same energy $3 - 1800$ hits. This can be explained using the knowledge that all the processes that occur are based on a probabilities, not only the chance whether the pion will decay, but also how the energy is distributed. Since we know that this energy is distributed between all the daughter particles, we know that the shower energy E_{shower} can be between the rest mass of a responsible particle, i.e. a photon and the total energy of the incoming particle E_{beam}, thus $0 < E_{shower} <= E_{beam}$.

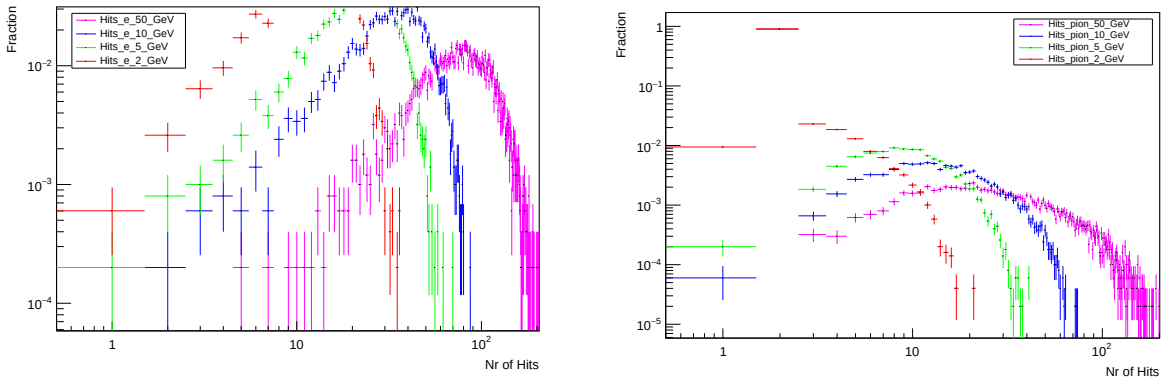

Figure 5: The distributions of number of hits for electrons and pions, respectively on the left and right hand side. These plots were made via a simulation without the incorporation of any charge sharing. In the pion plot we see that at there is a non-interaction peak, where the pion is unaffected. On the other hand we have a shower happening, since as we can clearly see that the one incoming particle leads to an excitation of up until ca. 1500 hits, and since we neglected any diffusion of the charge, this can only be due multiple particles, thus a shower.

From above observations and implications, we thus now know that a electron of these energies will certainly shower. This in contrast to a pion, for which most of them will not show any showering, and those that will, will primarily contain less energetic showers. This implies that we could determine a cut value, for which we identify an unknown particle as an electron if it has more hits than that value and as a pion whenever it has generated less. To see how well we can separate these two, we chose the cut value such that we have a 99% pion rejection or a 90% electron efficiency. These are respectively determined such that

$$\sum_{x=0}^{cut} p_{pion}(x) \geq 0.99, \tag{13}$$

where cut is the cut value and $p_{pion}(x)$ is the pion distribution and

$$\sum_{x=cut}^{\infty} p_e(x) \geq 0.9. \tag{14}$$

These cuts are drawn together with the hit distribution of pions and electrons in figure 6. From these cuts we see that the pion distribution increase faster in number of hits than the electron distribution does, as we can see from both just looking at the distributions, and the cut values, for we see that at 1 GeV the cut for the 90% electron efficiency is above the 99% pion rejection, implying that one would miscount less than 1% of the pions as electrons. This however flips at 5 GeV.
To have a more quantitative view on it, we will look at the pion rejection and electron efficiency, whenever we make a cut, using the other criteria. So what is the electron efficiency if we take a cut at 99% pion rejection and vice versa. These values are plotted in figure 7. As we can see from these plots, both the electron efficiency and pion rejection decrease. This implies that the distributions must show more overlap with each other, which was also concluded earlier from figure 6. We did not notice, however, that there was a large drop in the electron efficiency and pion rejection, implying a fast increase of the pion shower hits relative to those of the electron. This increase in overlap seems to reduce at the higher end of the plot, since we see that there is no longer a decrease in both plots.
Furthermore we see that the pion rejection even increases at the high momentum side, this could imply that the pion shower is stretched out over the whole 'spectrum'. This means that the side with a high number of hits increases approximately the same for both the pions and the electrons, while the lower end of the distributions increases faster for electrons than for pions. This behaviour seems to be confirmed by figure 5 and can be explained by the knowledge that the pion showers are distributed in energy.

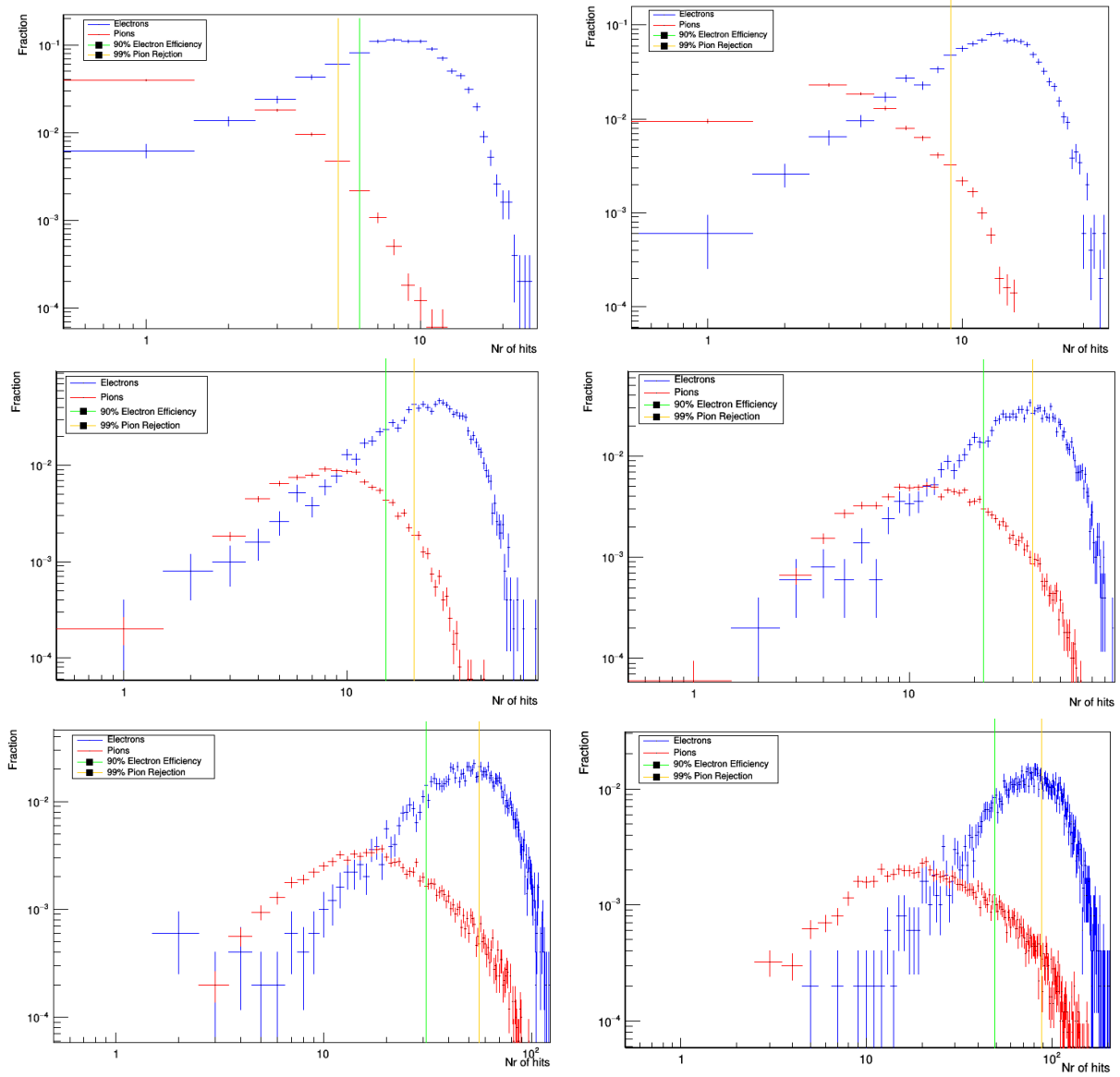

Figure 6: The electron and pion hit distributions, which are being superimposed per energy(Top left 1 GeV, top right 2 GeV, middle left 5 GeV, middle right 10 GeV, bottom left 20 GeV, bottom right 50 GeV). At every energy we have drawn a vertical line denoting the cut values for the given criteria. From this we can see that especially in the lower energy region, the number of hits of the pion shower increases faster than that of the electron shower, giving more overlap, and make it thus harder to separate.

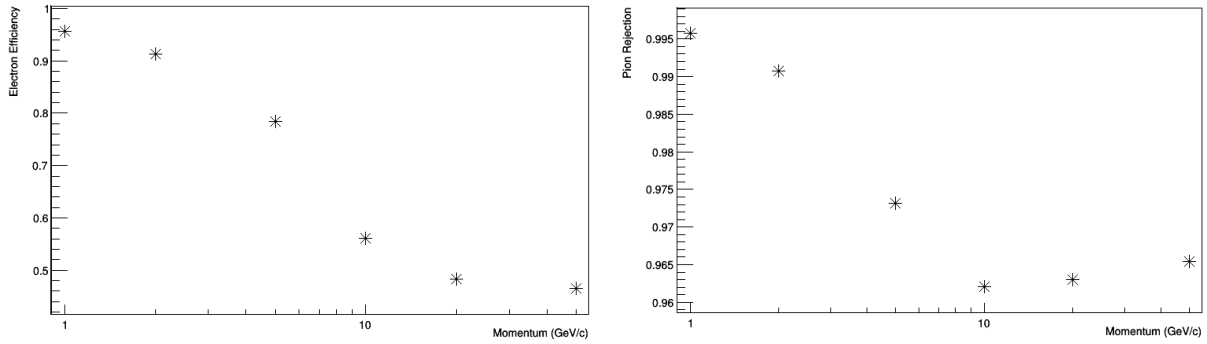

Figure 7: The electron efficiency (left) and pion rejection (right) as functions of the energy and at a cut of respectively 99% pion rejection and 90% electron efficiency, we have not includede the error bars, since these were hardly visible in the plot. As we can see from these plots, the separation between the two showers based on this technique is quite limited. For particles up to a momentum of 2 GeV less than 1% of the pions is mistaken for an electron and one loses up to 10% of the electrons. It also seems that at the higher energies the overlap between the two showers saturate, which can be explained using the knowledge that the pion shower can never be larger than its initial energy, which are approximately the same for both particles. The slight increase in only the pion rejection means that the pion shower must be stretching out instead of just moving, this seems to be confirmed by figure 5.

3.2.2 Charge Sharing

Now that we have found how the distributions behave in an ideal case, where every hit excites only one pixel. We will now look at a more realistic case, one where the charge is distributed the chip. As told before, we approximated this flow of charge as a Gaussian function. From this we found a distribution for one particle passing through a sensor, which was given in figure 4. Using the parameters used to create this distribution, we were able to construct the hit distributions in figure 8.
In these plots we can see that the electron hit distributions look quite similar to those we saw earlier in the case, where the charge was fixed at one position. This should idealy mean that

$$\langle N \rangle_{chargeSharing} = \langle N \rangle_0 \cdot \langle N \rangle_{ClusterSize} \tag{15}$$

with $\langle N \rangle_{chargeSharing}, \langle N \rangle_0, \langle N \rangle_{ClusterSize}$ the average number of hits for the case with and without charge diffusion and the cluster size respectively. The expected and calculated values are given in table 1. As we can see from these, for a small amount of hits, the values seem to approximately match, there are differences of only a few hits, while for the higher averages there are larger differences. This could be due to the residue charge that is still present in the active plane. This means that a pixel, which would not have enough charge to be activated due to one particle, could get enough charge to be activated due to more particles. On the other hand we have that whenever there are too much particles, they would have overlap in the pixels they would normally activate and as a result give less hits than expected.
The only clear difference for the electron distribution seems to be that the whole distribution is broadened from up until approximately 200 hits to up until approximately 800 hits. One could ask why there are only 800 hits and not many more, since it is possible to go up to $25 \cdot 200 = 5000$ hits. For this to happen, however, one needs all particles to excite 25 pixels, which as we can see from figure 4, already has a chance of almost zero to happen for a single particle. Even for every particle to excite more than 4 pixels has a chance of $0.05^{200} \approx 0$ to happen. So it is the most probable that every hit has up to 4 excitations per hit. Furthermore, the particles have to be far enough from each other such that there are as little overlapping pixels as possible and thus every pixel is registered. At last, we 'only' take 50.000 events, thus if some number of hits have a chance lower than $1/50.000 = 2 \cdot 10^{-4}$, it is quite probable that it is not found. Taking these arguments into consideration, it makes thus sense that there are 'only' 800 hits instead of 2500.
The pion distributions, however, look a bit different. Here it seems that there are two peaks instead of one. This can be explained as an artifact of non interacting pion peak we saw in figure 5. Namely, if we look at

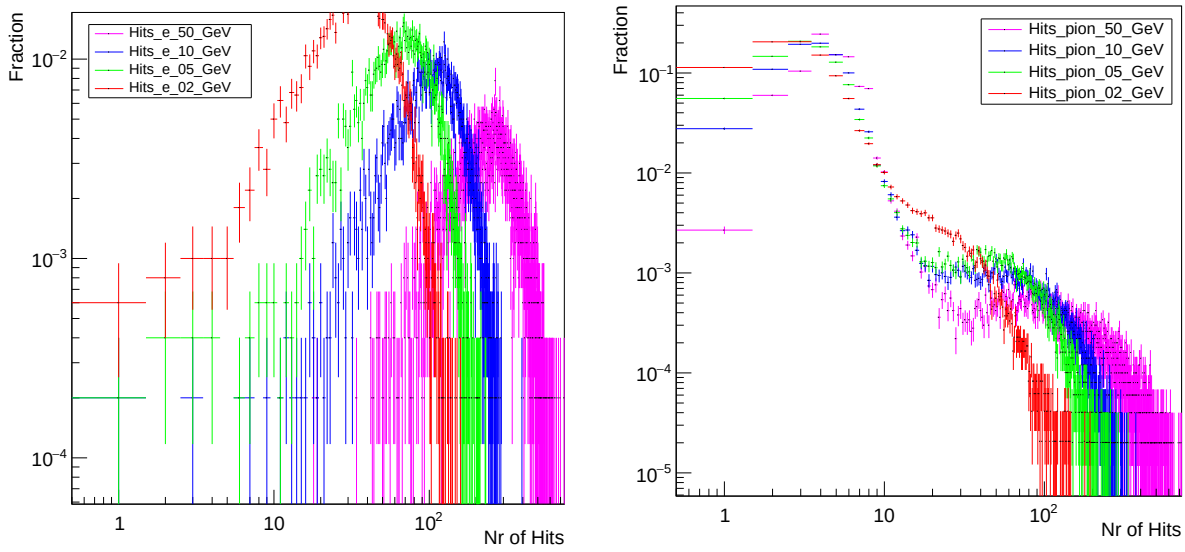

Figure 8: The distributions of number of hits for electrons and pions, respectively on the left and right hand side. These plots were made via a simulation, with the incorporation of charge diffusion. As we compare these to figure 5, we can see that the shape of the electron hit distributions have not significantly changed, there is only an increase in number of hits. The pion distributions have a bit changed, as there seem to be two overlapping Gaussian like distributions. These can be explained by considering twice the cluster size distribution from figure 4, since the first peak is every where the same and is thus a result of the non interacting pion, where as the other peak/shoulder is a result of the interacting and thus showering pions.

	Energy	$\langle N \rangle_0$	calculated $\langle N \rangle_{chargeSharing}$	calculated $\langle N \rangle_{chargeSharing}$
Pion	1 GeV	2.0	5.6	4.3
Electron	1 GeV	9.1	25.0	27.8
Pion	2 GeV	2.3	6.2	6.1
Electron	2 GeV	14.6	40.0	43.6
Pion	5 GeV	3.0	8.3	10.6
Electron	5 GeV	25.7	70.4	78.9
Pion	10 GeV	3.9	10.8	13.5
Electron	10 GeV	38.0	104.2	119.8
Pion	20 GeV	4.8	13.1	16.4
Electron	20 GeV	54.4	149.2	173.3
Pion	50 GeV	6.2	17.0	20.9
Electron	50 GeV	85.9	235.8	269.9

Table 1: The expected and measured average number of hits for the distributions of the charge sharing assumption. These expected number of hits were calculated using equation 15. As we see from this, for a low amount of hits, this approximately matches, but for higher hits there is an increasing deviation from it.

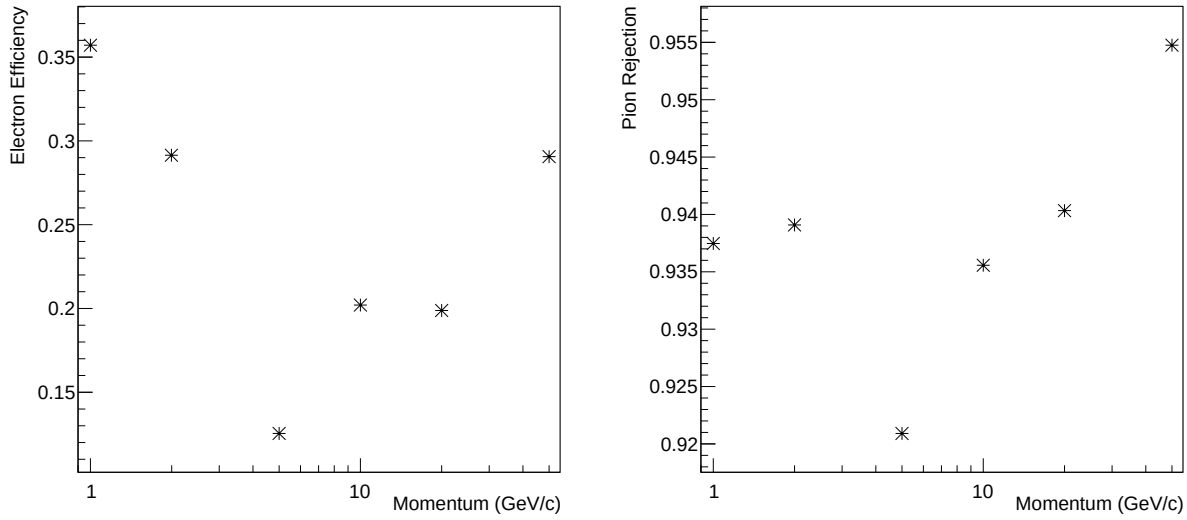

Figure 9: On the left the electron efficiency, when we set the cut at 99% pion rejection and on the right the pion rejection when cut a 90% electron efficiency. Comparing these to the previous non diffusing case, we notice that and the overall efficiencies/rejections went down and the shapes changed. The decrease in efficiency can easily be explained, since our 'orignal' distributions are smeared out by the charge diffusion, not every hit gives the same amount of signals. This will result in more overlap between the two distributions, thus a less efficient cut. The shape of these figures, however, are a bit harder to explain, for this, we need to look at the superimposed hit distributions in figure 10.

the hit distribution for two hits, we would find a chance of $0.15^2 \approx 10^{-2}$, which is the order of magnitude we find in our charge sharing distribution. Whenever you were to calculate the other probabilities as well, one would find the curve one sees on the side with a low number of hits in the pion distribution plot of figure 8. The tail or shoulder in this plot, however, cannot come from this non interacting pion, and thus it has to be due to the showering pions. As explained before, it should look like a spread out electromagnetic shower, meaning that the maximum number of hits should approximately coincide, while the minimum number of hits is lower. This is exactly what we see from the plots, where the number of hits for the 50 GeV pion shower is up until approximately 800 hits, which is the same as for the electron. However where the electron 50 GeV shower starts at approximately 30 hits, the pion shower seems to start even sooner.
With the understanding of these distributions, we can look at the behaviour of the electron efficiency and pion rejection when we respectively impose a 99% pion rejection and a 90% electron efficiency. These values are plotted in figure 9. As we compare these efficiencies with the ones we found earlier, we can see two important things. First of all, we see that the efficiency and rejection decreased significantly. This is due to the broadening of the distributions, which is caused by the distribution in number of signals per hit. This makes the distributions overlap more, such that we obtain a cut with less accurate properties.
Furthermore we see that the shape of these efficiency and rejection changed significantly. Previously in the case where there was no charge diffusion we saw a curve that had a slowly decreasing part in the beginning, then a drop and afterwards an approximately flat part. Here we see first a drop and then a rise. To understand this, we have to look at the distributions per energy, which are given in figure 10. In these plots we see that for the pions with a momentum below 5 GeV there is only one peak and a shoulder and between 2 and 5 GeV this shoulder breaks off and it forms its own peak, while lowering the peak of the non interacting pions. This lowering appears to be large enough to dominate the behaviour of the efficiencies, on the other hand, however, we notice, as we also did earlier, that the pion distribution is not a shower with a specific predetermined energy, but rather a distributed shower energy.

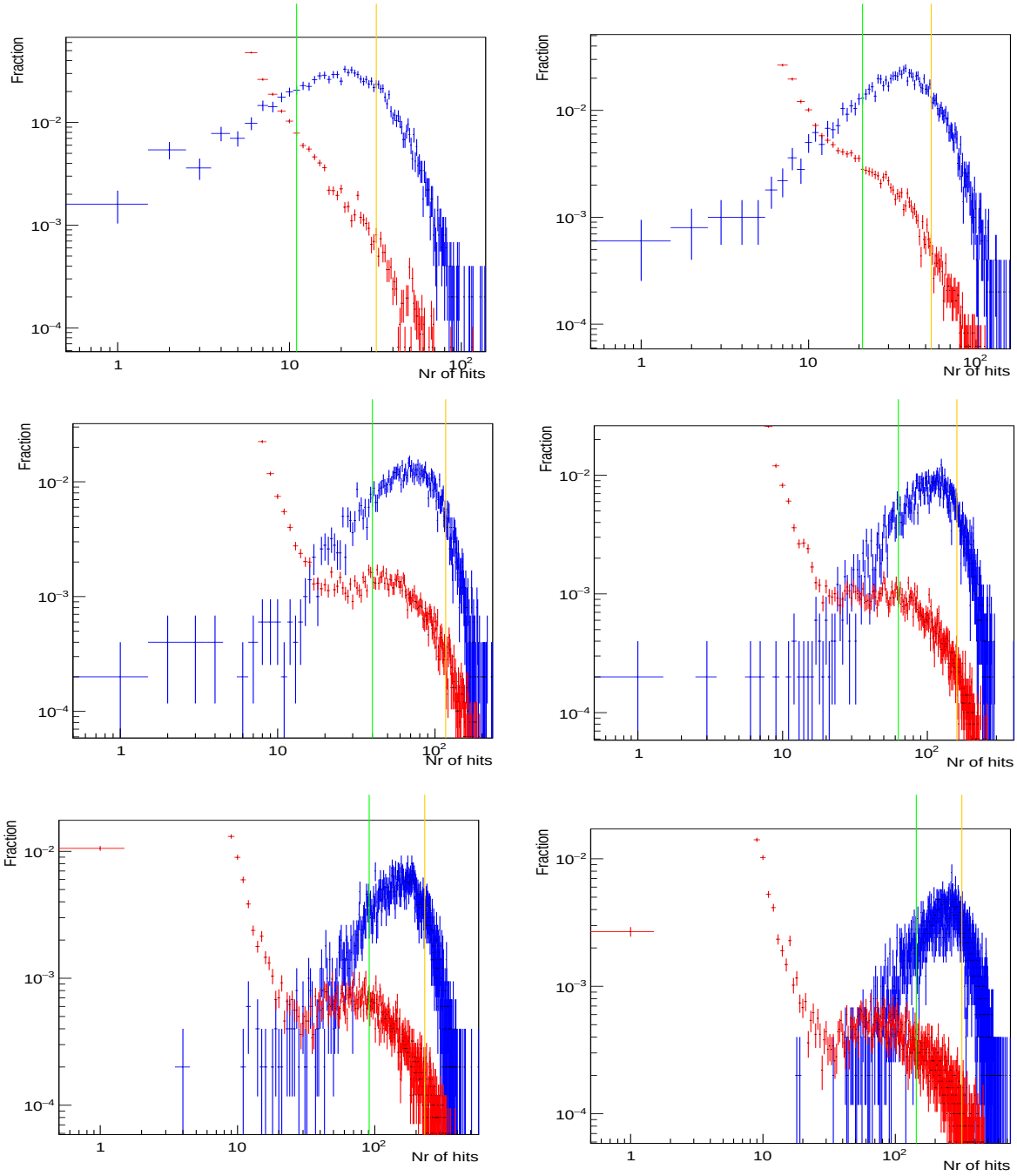

Figure 10: The electron and pion hit distributions, which are being superimposed per energy(Top left 1 GeV, top right 2 GeV, middle left 5 GeV, middle right 10 GeV, bottom left 20 GeV, bottom right 50 GeV) where blue indicates the electrons and red the pions. Furthermore the cut values are shown, yellow indicates the 99% pion rejection cut and green the 90% electron efficiency cut.

3.3 Discriminator settings

Now that we have seen what the distributions of hits look like and how they behave, we can try to improve our found accuracy. The ones we found, namely, were approximately $20 - 30\%$ electron efficiency at a 99% pion rejection and around 94% pion rejection at 90% electron efficiency. As we saw earlier when we went from a model without charge diffusion to a model with. the accuracy of the discrimination severely dropped. From this rises the idea to change the cluster size of one hit, this can be done by the change of two parameters, as we can see in equations 10 - 11. One is the width of the charge σ and the other is the discriminator value α. We could choose to look at the impact of changing the width of the charge distribution, however, to control this in a real experimental setup is extremely hard. For this it is not useful to look into it.
The other option, the discriminator can be more interesting. One could namely expect that for a higher discriminator value, the cluster sizes become smaller and with it they are being confined, this could lead to a better confined hit distribution, which could lead to a more accurate distinction between pions and electrons. First we will take a glance at the behaviour of the cluster distributions, these can be found in figure 11. In these plots we can see various things. First of all, we can see that the shape of the cluster size distributions does not seem to be so different, especially not in the tail area, which begins at a cluster of 5 pixels. it looks like there is a fast drop until a size of 15 and after that there is a plateau like area. It could also be that it will decay further, but we can only see up until a resolution of 10^{-4}. There is, however, one noticeable change, as we compare the values at a cluster size of 5, we can see that for $\alpha = 13$ there is a change to find it of approximately 310^{-2}, this drops to a chance of approximately 10^{-2}, thus it drops with approximately a factor 3. This same factor can be found when looking at the other cluster sizes. This is apart from the visual an indication that the shape in the tail area does not change significantly.
If we look at the area up until a 4 pixel cluster size, we see, however, that the shape significantly changes whenever we change the discriminator value α. There is nevertheless a certain pattern we can recognize in it. As we look through the plots we can see that the higher we choose our discriminator value, the lower the high value peaks become. This is easily explained by the fact that one needs a higher charge to be induced by the passing particle to excite the same pixel, see equation 10. This leads of course automatically to the rise in chance of finding a cluster of size one. We see, however that the 2 and 3 pixel sized clusters do not rise or fall as fast as the 1 and 4 sized clusters. This is due to the balance in gaining and losing cases.
This same effect also leads to another issue, we lose hits. As we see in the plots, there are 9974 entries in the $\alpha = 13$ case and decreases to 8629 entries for $\alpha = 18$. This could be a potential problem to discriminate electrons prom pions, since our method is based on counting the number of hits as exact as possible. If we only count a fraction of this, we will lose data and with it, we will probably have a less clear distinction between the two hit distributions. This could be countered by the contraction of the cluster size distribution, but as we discussed earlier, there are visually no clues that this is happening. There is another more quantitative clue this does not happen, whenever we look at the standard deviation of the distribution, we can see that this does nearly not change at all. In every distribution it is around 1.5 with only marginal deviations.
When we implement these different discriminator values, we find that the distributions look approximately the same, for this to see it is sufficient to look at the most extreme case, the case whit a $\alpha = 18$. The found hit distributions are given in figure 12. When we compare these to our previously found distributions, for a default discriminator value of $\alpha = 14$, we see that there are apart from the total number of hits, which decreased a bit, not really many changes visible. Only if we look closely to the pion distribution, we can notice that the distinction between the two peaks has lessened. This is due to the chance that we do not detect hits, as we saw in the cluster size distributions, these distributions shifted to the small cluster sizes, while the tail remained apart from its height reasonably the same, this leads obviously to a shift of the showering peak to the non interacting peak, while the right hand side of the non interacting peak remained on approximately the same position. This clearly leads to a contraction between both peaks.
To see how the electron efficiencies and pion rejections effectively change, we take a look at these for the discriminator settings $\alpha = 14$(default),$\alpha = 15$and$\alpha = 18$, these are respectively given in figures 9, 13 and 14. Whenever we compare these, we see that when the electron efficiency seems to change about 0.05, when we make a jump from the default discriminator to one higher. These drop even more when we go to even higher values of α. For the pion rejection, however, these changes are more marginal and only on the order of 0.01. There is an odd behaviour, however, when we look at the high momenta range, we see that both the electron efficiency and the pion rejection, do not show such a drop. They seem almost to be unaffected by those. This is probably due to the statistics, after all, we made the assumption earlier that this drop would

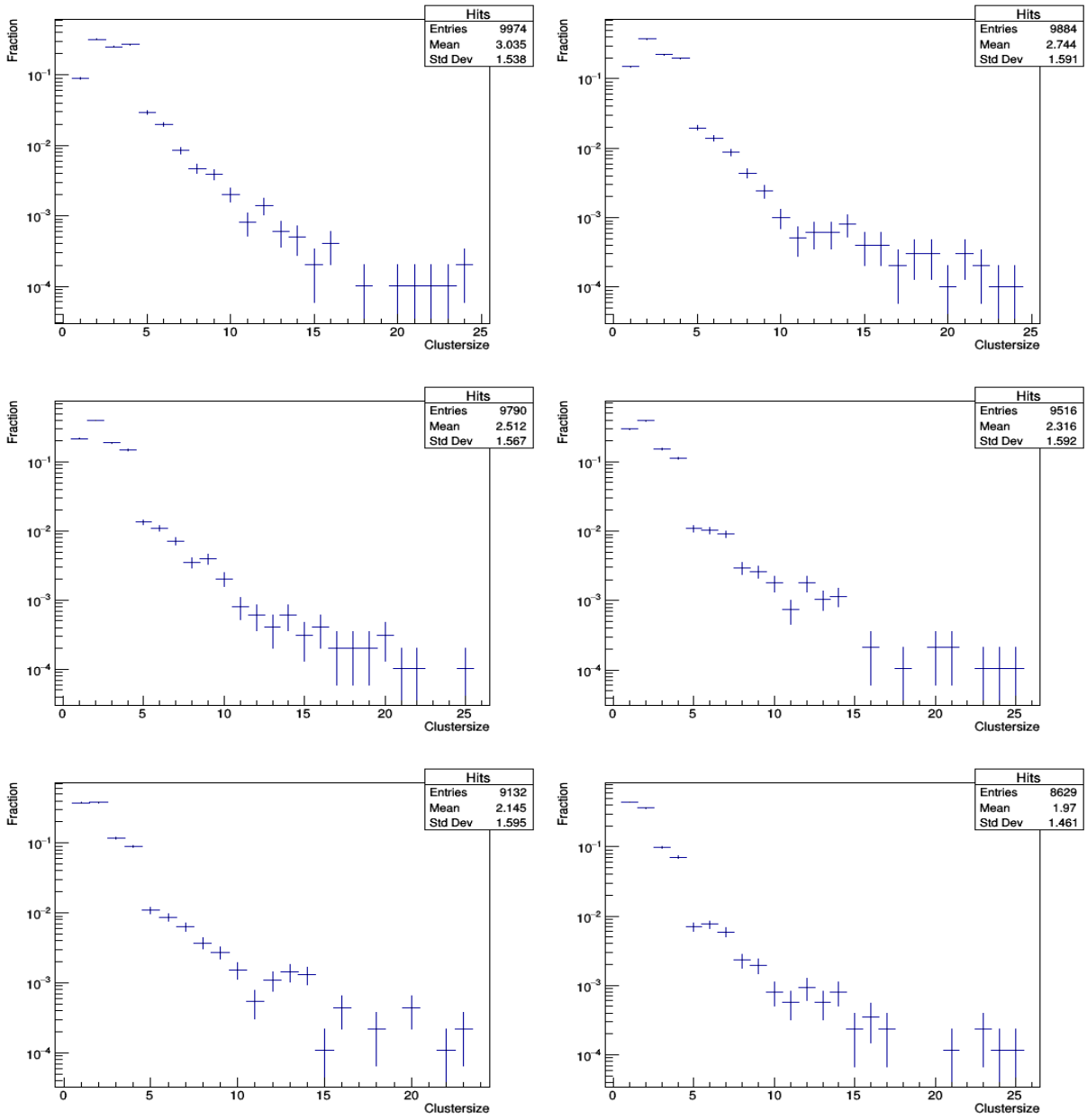

Figure 11: The different cluster size distributions, where we have varied the discriminator value α. The used values were 13 (top left), 14 (default, top right), 15 (middle left), 16 (middle right), 17 (bottom left) and 18 (bottom right). For every simulation we used $10,000$ events, thus we can see from the number entries that the higher we set the discriminator value, the less hits are measured. Furthermore, we see that the shape of the distribution does not change significantly, in every plot we namely see a tail, which looks approximately the same, the only difference is that it lowers a bit. The standard deviation does not show a very clear change, all are in the order of 1.5, which indicates that the distribution does not confine. The only obvious change we notice is in the region of $1-4$ hits, where the we see that the larger sizes lower in height and the smaller ones raise.

come from the decreasing number of measured hits. If this is indeed the underlying reason, it seems to be that it is enough to count a fraction of the total number of hits. In other words, the non interacting peak is well enough separated from the showering one to be affected by any change of discriminator.

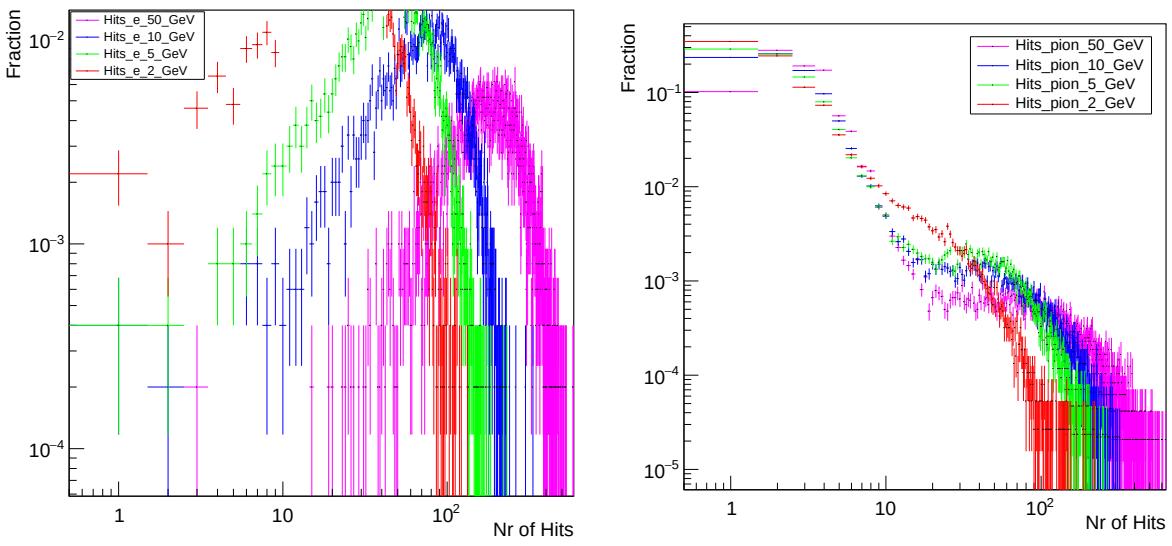

Figure 12: The hit distributions for the electrons on the left hand side and the pions on the right hand side. These are for a system where we set the discriminator value $\alpha = 18$. When we compare these with our previous case for a discriminator of $\alpha = 14$ (figure 8), we notice that for the electrons the hit distribution does barely change apart from the decrease in number of hits. The pion distribution has changed another aspect, due to the decrease in number of hits, the overlap between the two separate distributions has increased a bit.

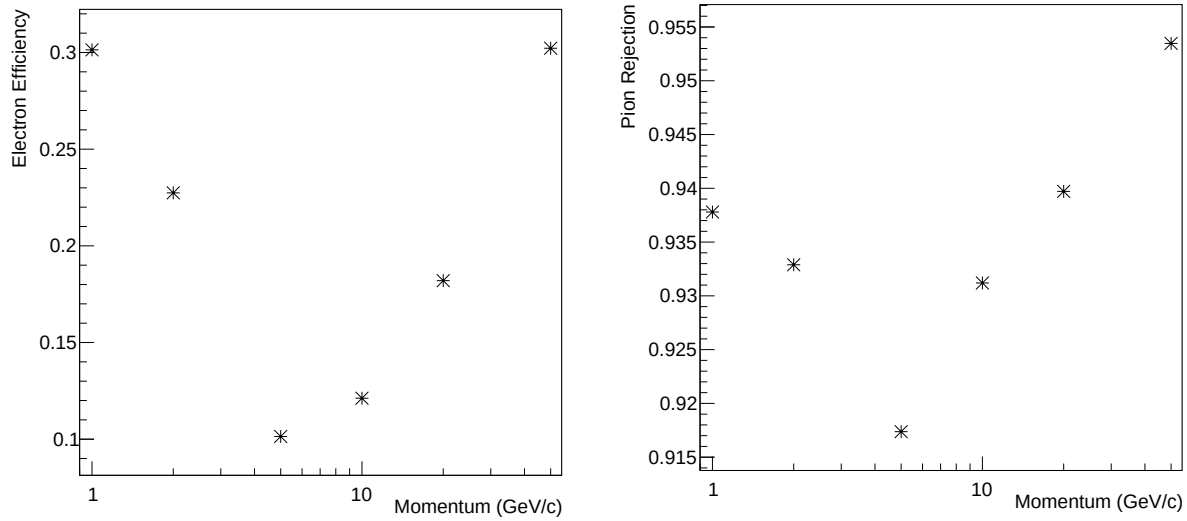

Figure 13: The electron efficiency on the left and the pion rejection on the right for a detector with a discriminator value of $\alpha = 15$. The electron efficiency was determined by a cut for a 99% pion rejection and the pion rejection for a 90% electron efficiency. As we see from these plots, compared to figure 9, the electron efficiencies went down with about 0.05 and the pion rejections stayed approximately the same.

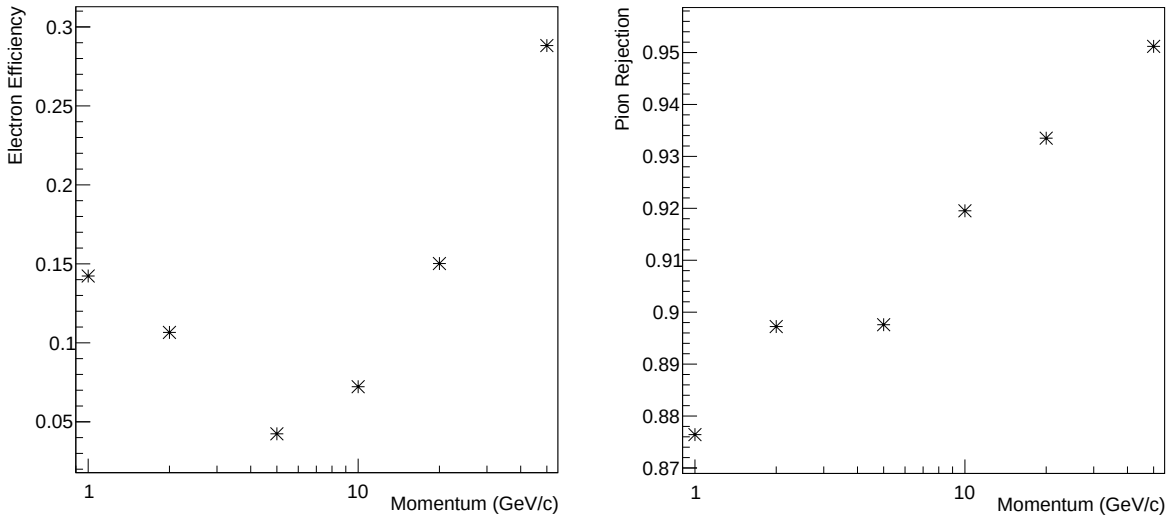

Figure 14: The electron efficiency on the left and the pion rejection on the right for a detector with a discriminator value of $\alpha = 18$. The electron efficiency was determined by a cut for a 99% pion rejection and the pion rejection for a 90% electron efficiency. As we compare this to figure 9 and 13, we see that both the efficiencies and rejections went down even further. We can thus safely conclude that raising the discriminator will not improve our results.

3.4 Configuration settings

Now that we have seen that changing the discriminator will not improve the distinction between the pions and electrons, we will have to look for another way. Another easy way that one can alter in an experiment is obviously the geometry of the detector. To look at this systematically, we will look at the cases where there are equally stacked layers. These layers will consist of a 0.4 cm thick block of tungsten, with behind it a 2.8 µm thin layer of silicon. Since it is supposed to be a preshower detector, we will only look up until 5 of these layers. The hit distributions of the most 'extreme' cases, the 1 and 5 layers cases, can be found in figure 15.

As we can see in these plots, the shape of the distributions look quite similar as earlier. Even for the two peaks in the pion hit distributions we see that the overlap stays relatively the same. The onl;y clear difference between them, can be seen in the electron distribution plot. Looking at those, we namely see that in the simulations with only 1 layer the different energies are barely separated. This changes when we go to 5 layers, where every peak is claerly visible.

This makes sense, since more layers provide us with more data. More data, obviously means that we will have less statistical fluctuations. This together with the fact that a more energetic shower will produce more particles, gives a better separation. This is exactly what we when we look at those distributions.

This is not directly of importance to us, but as we saw before, the pion hit distribution is partially due to the showers of a distributed energy, this implies that the lowest energies of the showers will be sufficiently low that they will not or will barely overlap with the electron hit distribution. This would mean that we gain a higher accuracy when performing a cut. In other words, we suspect that the geometries with more layers have higher pion rejection and electron efficiency values. These are plotted in figures 16 and 17.

From these plots we can see a few things, looking at the y-axis we see immediately that that the range increases. This implies that the distributions are indeed better separable, when we increase the number of layers as we suspected earlier. We also see what the approximate values are that one is able to accomplish with only using this method. For a single layer for example, we see that we only have a few percent electron efficiency for a pion rejection of 99%. We also see that we reject less than 90% of the pions for a 90% electron efficiency. This implies that even the non interacting pion distribution peak overlaps with the electron distribution peak, which one can also see back in figure 15. This means that one layer will certainly not

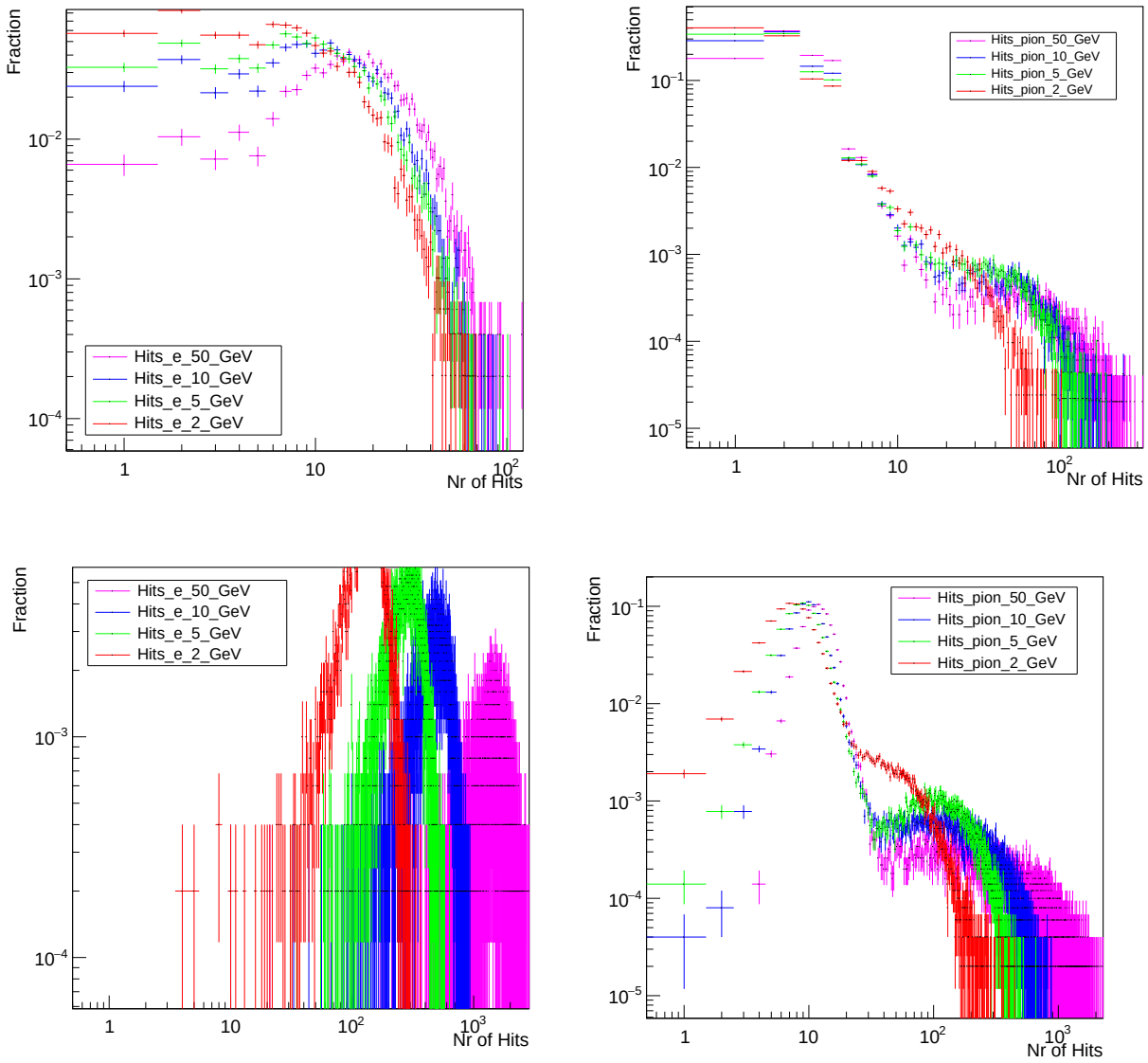

Figure 15: The electron (left plots) and pion (right plots) hit distributions for a thickness of 1 (upper plots) and 5 (lower plots) layers. Whenever we compare these, we see that apart from the number of hits, both distributions look very similar in shape. The only noticeable change seems to be the seperation between the different energies.

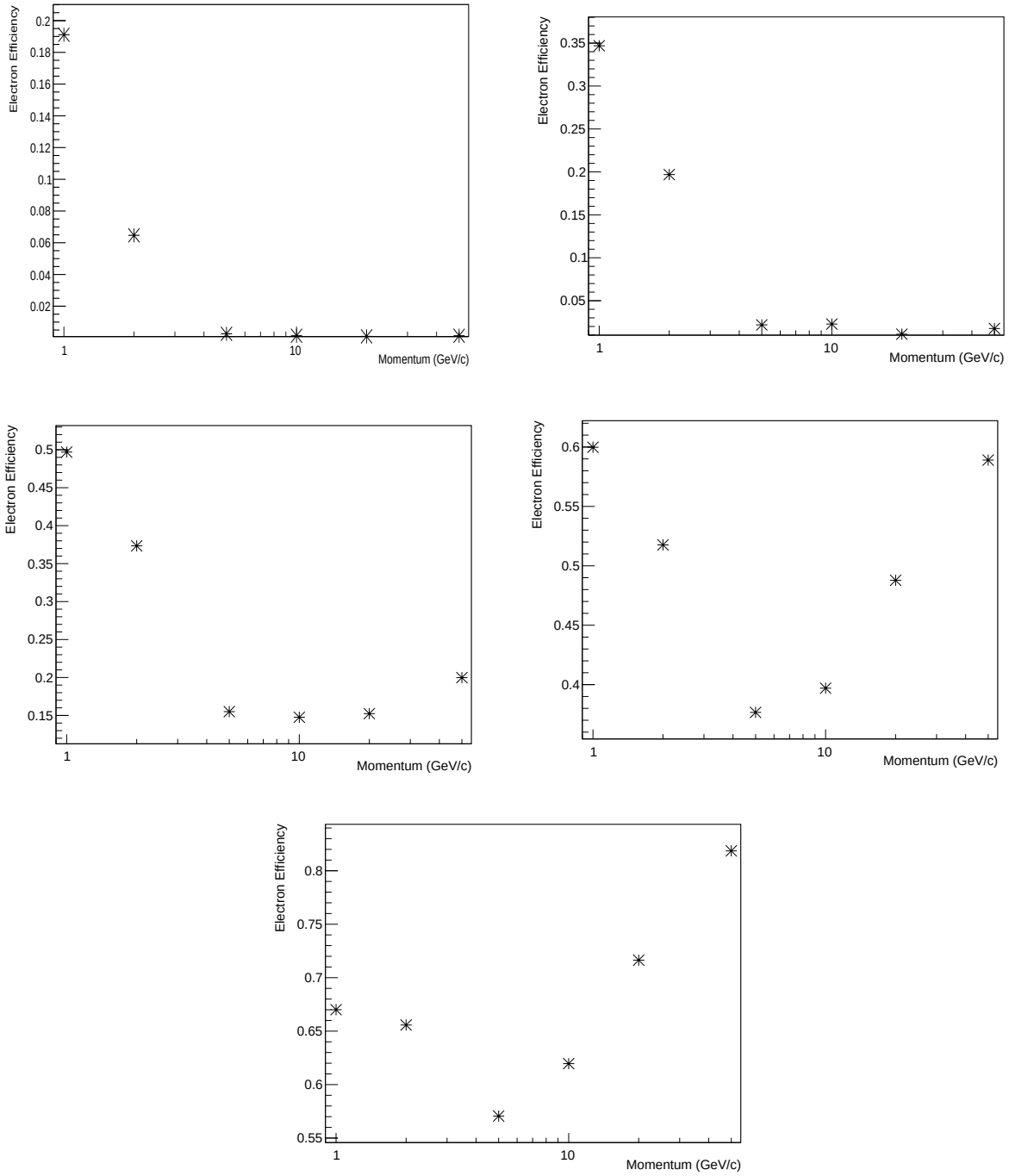

Figure 16: The electron efficiency against momentum for 1 (top left), 2 (top right), 3 (middle left), 4 (middle right) and 5(bottom) layers. In these plots we can indeed see that the efficiency increases significantly when we add more layers, which is exactly what we would have expected. Furthermore we see that the overall shape stays the same, only for the cases where there are just a few layers, there seems to be a deviation from it, this could be due to the very low efficiencies.

work. The best option seems to be the 5 layered system and possibly it improves even further when we add even more.

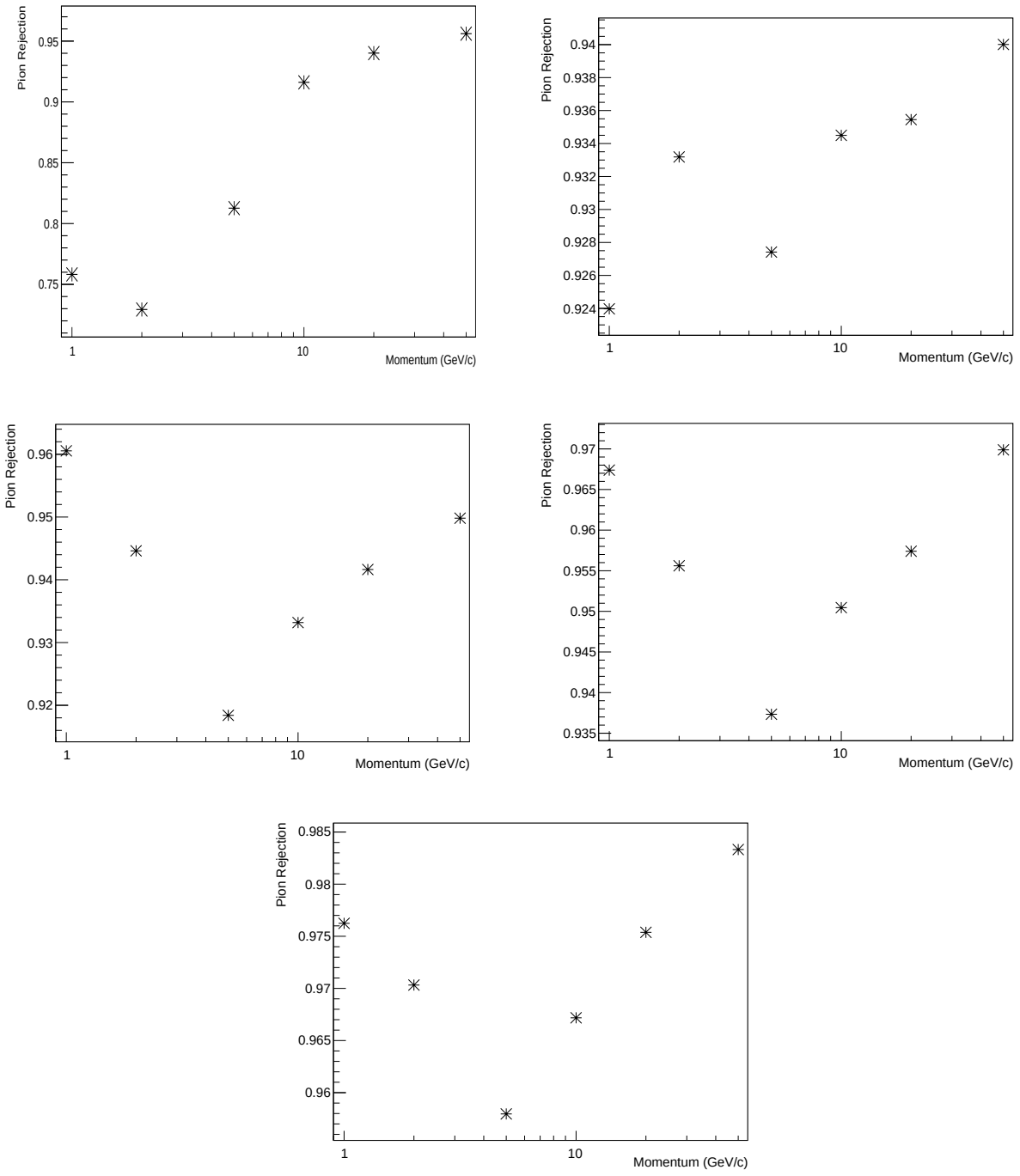

Figure 17: The pion rejection against momentum for 1 (top left), 2 (top right), 3 (middle left), 4 (middle right) and 5(bottom) layers. Here we can see the same behaviour as for the electron efficiency, the fraction pions rejected keeps increasing, which indicates that the pions and electrons can be separated better. Furthermore, there seems to be a common behaviour

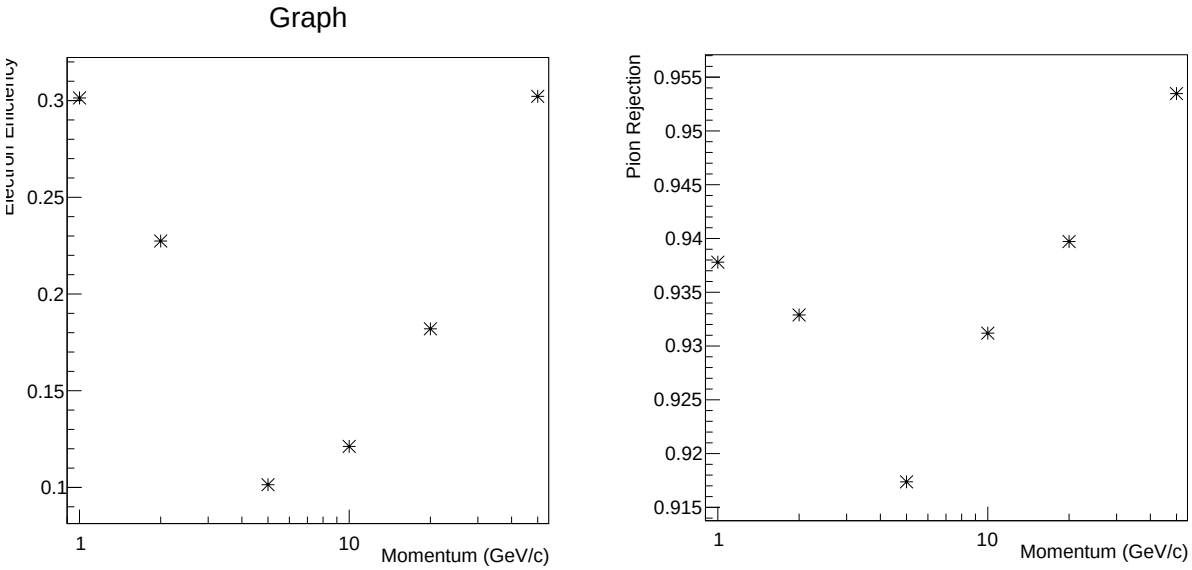

Figure 18: The electron efficiency and pion rejection for the same simulation as in figure 9, as we can see, there are some clear differences. The most obvious ones are the shape, where the 10 GeV point was in the previous electron efficiency plot about the height of the 20 GeV particles, here it is far lower. Furthermore the y-axis have dropped with about 0.5.

3.5 General Remarks

Although it looks very promising, there are some general remarks to be made. First of all, we used a geometry, which was nothing more than a thick block of tungsten with a thin layer of silicon behind it. This means we have neglected the electronics, the glue and other minor stuff. As we saw in section 1, this could lead to for example to more transition radiation, thus a slightly different shower hit distribution. We do not expect, however, this will significantly affect our results or at least will not worsen the results we found, since the layers are very thin and if there is a chance that it will produce more particles, this effect will be larger for a larger shower, since there are more particles passing through. This would mean that a larger shower will move to the right even more, making the pion distribution spread out even more and with it the separation between the two hit distributions will be even better.

Another approximation was that, although we used the area of four chips, we have implemented it only as a single chip. In the real detector, these four chips cannot be aligned such that you measure the hits exactly, either there is some space between them and particles pass in between, or either the chips are aligned with some overlap and you measure each particle twice. Both these cases will introduce some higher uncertainties in the number of passing particles for the central area, meaning that both the hit distributions will probably spread a little, which will lead to lower accuracies. This overlap or gap between the two chips, however, will be only in the area between the chips and has a width of only a few pixels, so probably this will not hurt the accuracies very much.

As we can see in figures 16 and 17, there are some points that seem to be in the wrong position. For example the pion rejection of the 1 GeV particles for the 2 layered system. Looking at the other plots, we notice that this point should probably be above the point at 2 GeV, which is clearly not the case. A possible explanation is that we made a wrong assumption regarding the error bars. To see whether this conclusion is right we performed another simulation for the first case as described in section 3.2.2. These results are plotted in figure 18. As we can see from this, there are some data points that seem to be in different positions, for example the electron efficiency for 10 GeV particles. This gives a clue that we indeed did not implement the right errors. But if we look at the absolute fractions, we can estimate our error for the electron efficiency to be on the order of 0.05. For the pion rejection it seems to be about 0.005. This means that the values we found are not as reliable as we would wish, but the quantitative arguments still hold, since the differences between the cases seemed to be large enough.

4 Conclusion

To summarize the results shortly, we found that all electrons will shower, this in contrast with the pions of which approximately 10% will shower and the rest will remain untouched. Secondly we noticed that whenever we added a distribution of the induced charge, rather than an singularity, the pion hit distribution splits in two different overlapping Gaussian-like distributions. Furthermore we saw an undesirable effect, the distributions of the pion and the electron show a lot of overlap, making it severe worse to discriminate the one from the other. We tried to improve this with raising the discriminator value above which charge a pixel is activated, this, however, did not improve the results, in fact the results were even worsened. In other words a higher discriminator value than the default value gives rise to two more overlapping distributions. At last we looked at the impact of the amount of layers, for this we saws that the more layers we had, the more accurate we were able to discriminate electrons from pions.
This brings us to the conclusion that one wants to have as many layers as possible and is able to count up to $55 - 80\%$ of all the electrons for a pion rejection of 99% using a 5 layered system.

4.1 Further Research

This was only the tip of the iceberg, regarding the search for a good preshower detector. We for example only looked at the bare hit distributions, one could for example also look at the depth of the shower, it could for example be that a part of the pion showers that show overlap with the electron showers can be excluded, because they began to shower later. Furthermore, one could also look at the shape and width of the showers and if they differ.
One can, however, also improve these results further. As we told before we have probably made an error regarding the errors. To obtain more reliable outcomes, one can search for another way to calculate those, for example, one could implement an error in the cut value, which was simply not done. Other improvements to be made, are a more quantitative view on the development of the showers, one could for example look whether the RMS over mean really changes for an increasing number of layers. One could also have a brief look at the impact of a smaller discriminator value, since we only had a look for the larger values, so this might improve the results a bit.
There are some other interesting features that have not been covered, for example one could look at the behaviour of the cut values themselves and see if there is any way to predict it for a certain momentum. Apart from this, one could also look whether the chosen criteria are the best, or that there is a more efficient one, this can for example be done by plotting the pion rejection as a function of the electron efficiency and find the point where both are as high as possible.
At last there are some improvements to be made in the used code and geometry. As told before, we approached the geometry of the detector as a simple block-like structure, this is, however, not completely realistic. One would preferably have a geometry, which includes the electronics and different chips. The code itself is not as efficient as it can be, the charge diffusion for example has to calculate the Gaussian for every hit, this can be rewritten by an approximation where the Gaussian is only calculated for some different positions within the pixel and placed in a look-up table.

References

[1] Peter-Jan Blenkers. "The development of a GEANT based Monte Carlo simulation framework for the R&D process of the FoCal calorimeter". MA thesis. Utrecht University, Aug. 2012.

[2] B.R.Martin. *Nuclear and Particle Physics*. 2nd ed. London: Wiley, 2009. ISBN: 978-0-470-74274-4.

[3] Panos Christakoglou. "Interaction of particles with matter, detectors, accelerators". URL: `https://surfdrive.surf.nl/files/index.php/s/yr8zE9EfW6OZl1R#pdfviewer`.

[4] D.W.Ball. *Physical Chemistry*. 2nd ed. Stamford: Cengage Learning, 2015. ISBN: 978-1-133-95843-7.

[5] D. Adamová *et al. A next-generation LHC heavy-ion experiment*. arXiv:1902.01211v2. May 2019.

[6] Martijn Reicher. "Digital Calorimetry Using Pixel Sensors". PhD thesis. Utrecht University, Mar. 2016.

[7] Chunhui Zhang. "Measurements with a High-Granularity Digital Electromagnetic Calorimeter". PhD thesis. Utrecht University, May 2017.

A Distributions for different geometries

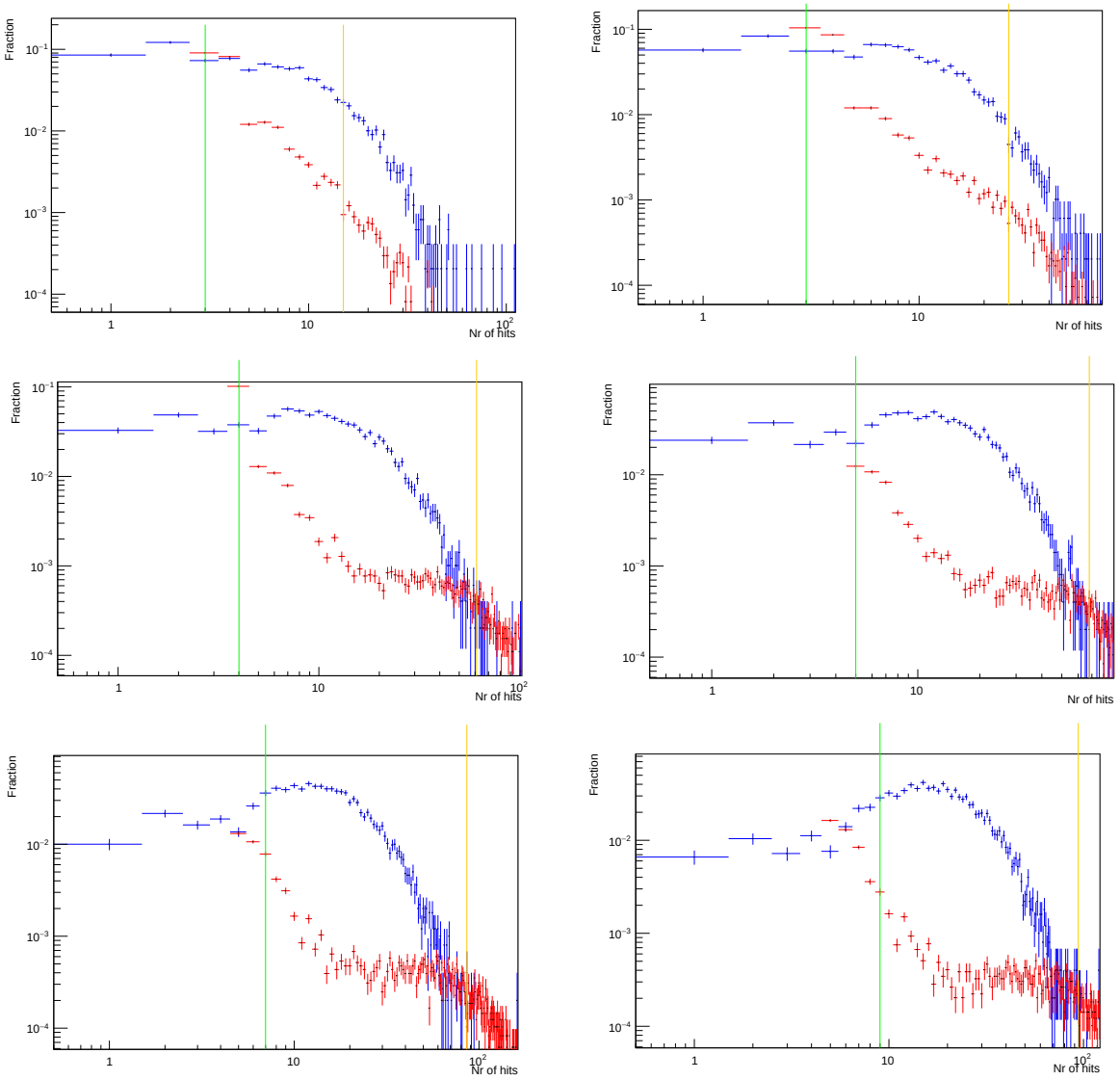

Figure 19: The electron and pion hit distributions, which are being superimposed per energy(Top left 1 GeV, top right 2 GeV, middle left 5 GeV, middle right 10 GeV, bottom left 20 GeV, bottom right 50 GeV). These are drawn for a 1 layered system. The yellow line indicates the cut value for 99% pion rejection and the green line indicates a 90% electron efficiency.

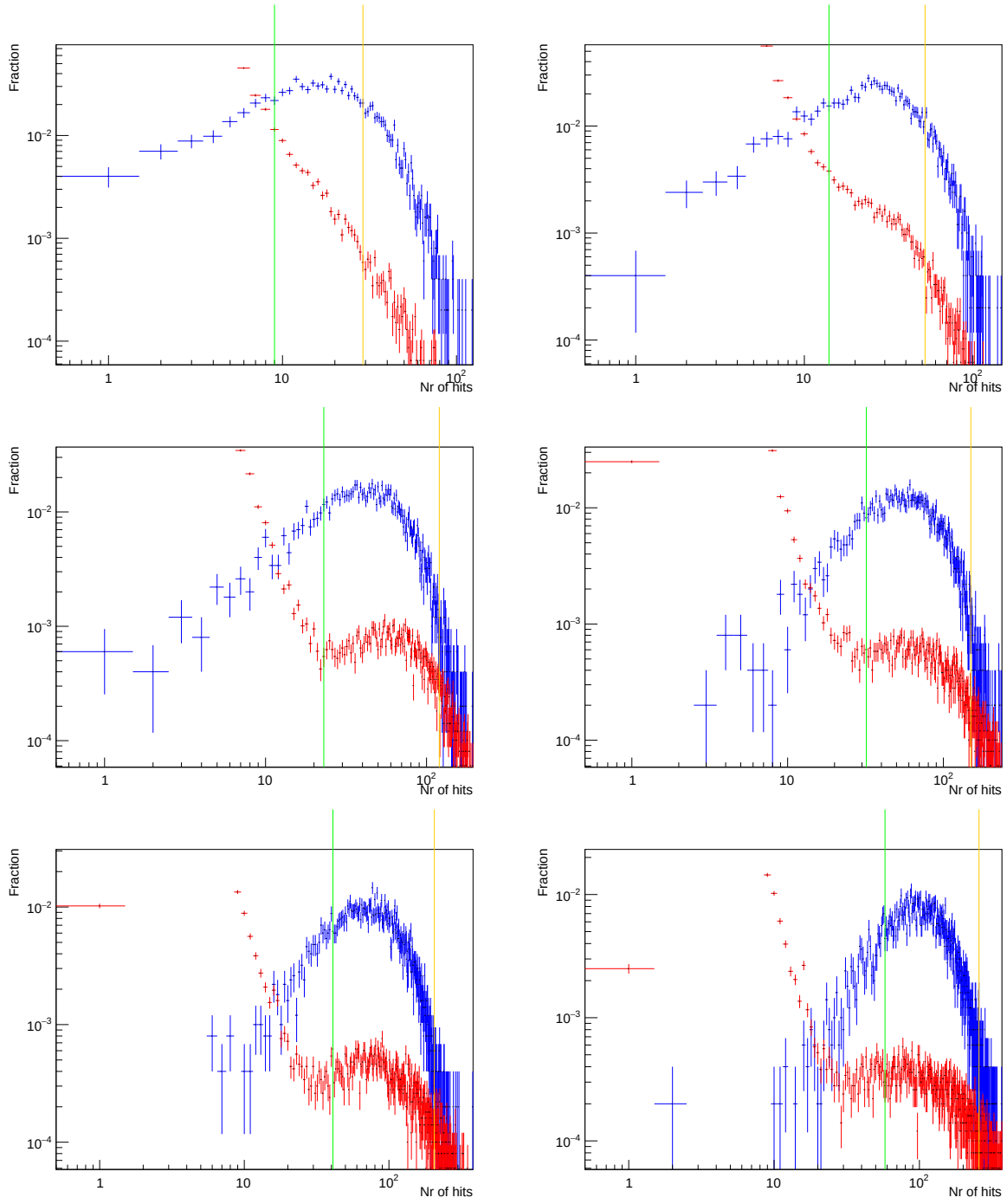

Figure 20: The electron and pion hit distributions, which are being superimposed per energy(Top left 1 GeV, top right 2 GeV, middle left 5 GeV, middle right 10 GeV, bottom left 20 GeV, bottom right 50 GeV). These are drawn for a 2 layered system. The yellow line indicates the cut value for 99% pion rejection and the green line indicates a 90% electron efficiency.

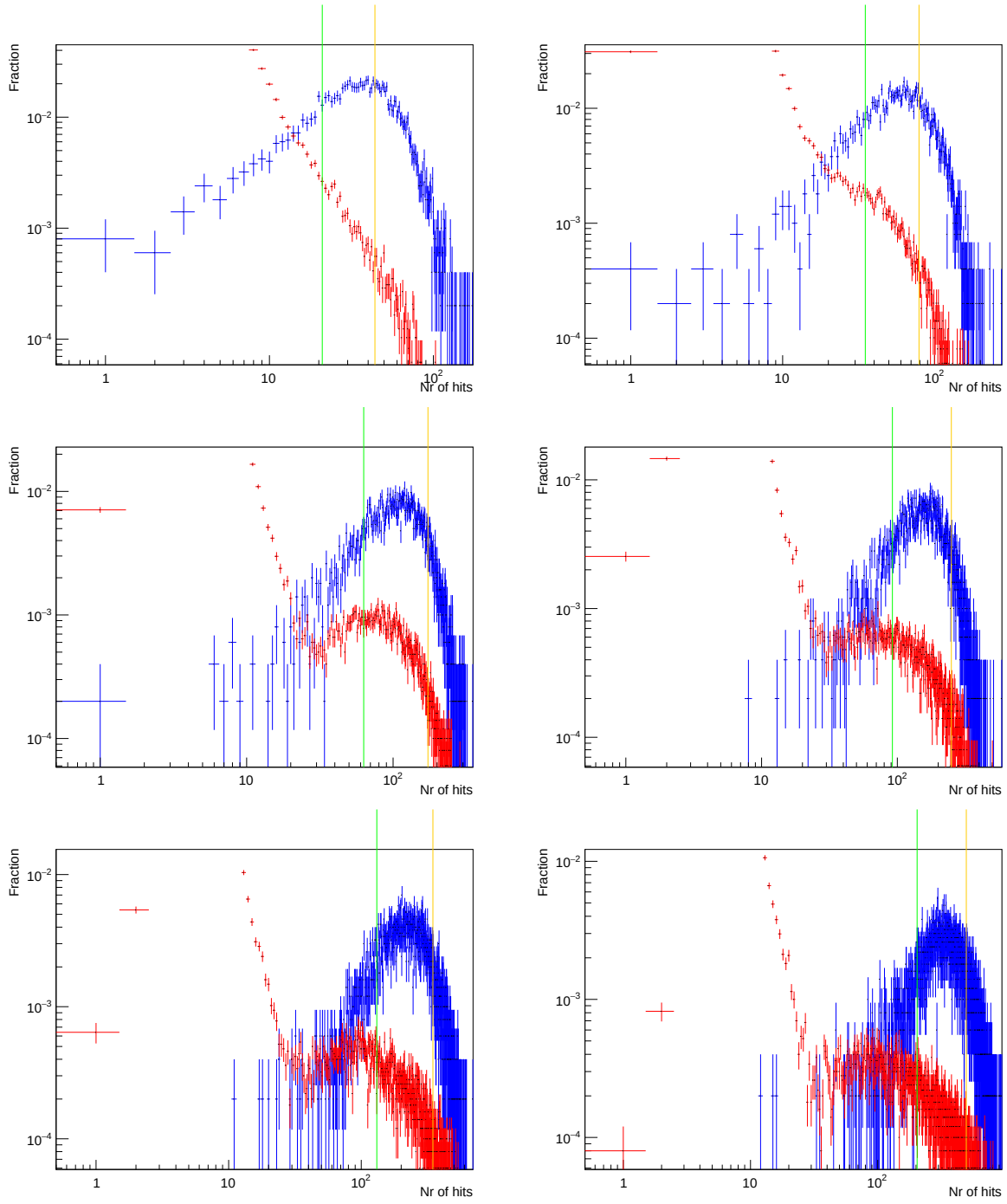

Figure 21: The electron and pion hit distributions, which are being superimposed per energy(Top left 1 GeV, top right 2 GeV, middle left 5 GeV, middle right 10 GeV, bottom left 20 GeV, bottom right 50 GeV). These are drawn for a 3 layered system. The yellow line indicates the cut value for 99% pion rejection and the green line indicates a 90% electron efficiency.

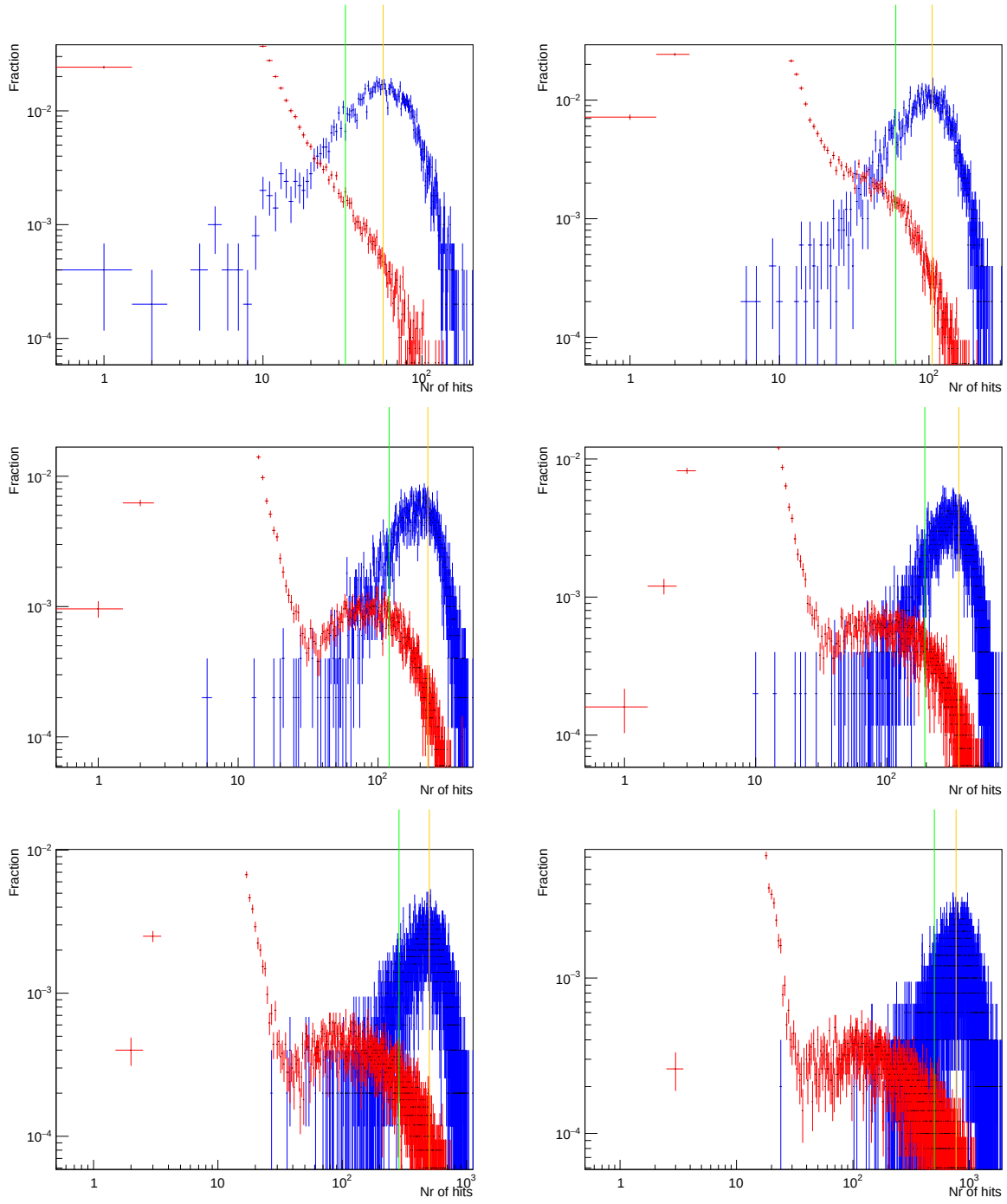

Figure 22: The electron and pion hit distributions, which are being superimposed per energy(Top left 1 GeV, top right 2 GeV, middle left 5 GeV, middle right 10 GeV, bottom left 20 GeV, bottom right 50 GeV). These are drawn for a 4 layered system. The yellow line indicates the cut value for 99% pion rejection and the green line indicates a 90% electron efficiency.

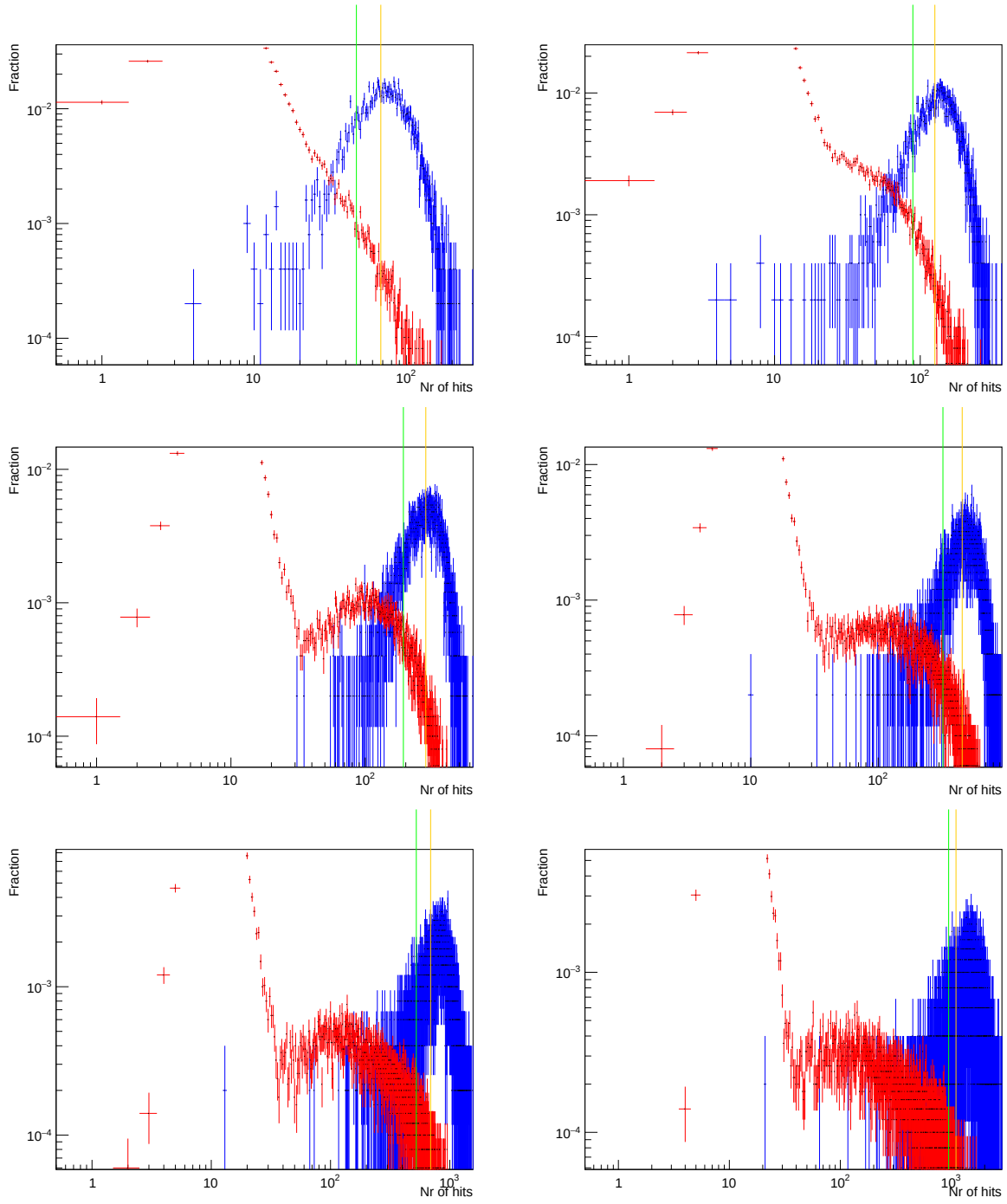

Figure 23: The electron and pion hit distributions, which are being superimposed per energy(Top left 1 GeV, top right 2 GeV, middle left 5 GeV, middle right 10 GeV, bottom left 20 GeV, bottom right 50 GeV). These are drawn for a 5 layered system. The yellow line indicates the cut value for 99% pion rejection and the green line indicates a 90% electron efficiency.